Brain, Behavior, & Immunity - Health 31 (2023) 100656

Contents lists available at ScienceDirect

Brain, Behavior, & Immunity - Health

journal homepage: www.editorialmanager.com/bbih/default.aspx

Parkinson's disease relevant pathological features are manifested in male Pink1/Parkin deficient rats

Benjamin G. Lamberty [1], L. Daniel Estrella [1], Jane E. Mattingly, Katy Emanuel, Andrew Trease, Steven Totusek, Lexi Sheldon, Joseph W. George, Mohannad A. Almikhlafi, Trey Farmer, Kelly L. Stauch [*]

University of Nebraska Medical Center, College of Medicine, Department of Neurological Sciences, Omaha, NE, USA

ARTICLE INFO

Keywords:
Alpha-synuclein
Motor symptoms
Neurodegeneration
Parkin/Pink1
T cells
Tremor

ABSTRACT

Animal disease models are important for neuroscience experimentation and in the study of neurodegenerative disorders. The major neurodegenerative disorder leading to motor impairments is Parkinson's disease (PD). The identification of hereditary forms of PD uncovered gene mutations and variants, such as loss-of-function mutations in PTEN-induced putative kinase 1 (Pink1) and the E3 ubiquitin ligase Parkin, two proteins involved in mitochondrial quality control, that could be harnessed to create animal models. However, to date, such models have not reproducibly recapitulated major aspects of the disease. Here, we describe the generation and phenotypic characterization of a combined Pink1/Parkin double knockout (dKO) rat, which reproducibly exhibits PD-relevant abnormalities, particularly in male animals. Motor dysfunction in Pink1/Parkin dKO rats was characterized by gait abnormalities and decreased rearing frequency, the latter of which was responsive to levodopa treatment. Pink1/Parkin dKO rats exhibited elevated plasma levels of neurofilament light chain and significant loss of tyrosine hydroxylase expression in the substantia nigra pars compacta (SNpc). Glial cell activation was also observed in the SNpc. Pink1/Parkin dKO rats showed elevated plasma and reduced cerebrospinal levels of alpha-synuclein as well as the presence of alpha-synuclein aggregates in the striatum. Further, the profile of circulating lymphocytes was altered, as elevated $CD3^+CD4^+$ T cells and reduced $CD3^+CD8^+$ T cells in Pink1/Parkin dKO rats were found. This coincided with mitochondrial dysfunction and infiltration of $CD3^+$ T cells in the striatum. Altogether, the Pink1/Parkin dKO rats exhibited phenotypes similar to what is seen with PD patients, thus highlighting the suitability of this model for mechanistic studies of the role of Pink1 and Parkin in PD pathogenesis and as therapeutic targets.

1. Introduction

Parkinson's disease (PD) is a prevalent, chronic, and progressive neurodegenerative disorder that affects 1–3% of the population over 60 years of age worldwide (Miller and O'Callaghan, 2015). Clinically, PD is characterized by motor symptoms including bradykinesia, rigidity, resting tremor, and postural instability. Pathologically, PD is characterized by the loss of dopaminergic (DA) neurons in the substantia nigra pars compacta (SNpc) and the presence of eosinophilic inclusions known as Lewy bodies containing alpha-synuclein (α-syn) and ubiquitin (Hirsch et al., 2016; Klein and Westenberger, 2012). This loss in SNpc DA neurons leads to a reduction in the release of dopamine in the striatum; as an outcome, motor symptoms of PD become apparent (Exner et al., 2012; Hirsch et al., 2016). Along with α-syn, neurofilament lightchain (NfL) considered a marker of axonal damage in a variety of acute and chronic neurological diseases, has become a promising candidate as a cerebrospinal fluid (CSF) and plasma biomarker for alpha-synucleinopathies, including PD (Canaslan et al., 2021; Quadalti et al., 2021), and might predict disease progression in dementia with Lewy bodies (Pilotto et al., 2021a). There are two forms of PD: sporadic, with likely multiple gene and environmental causative factors; and familial, genetically inherited in either autosomal recessive or dominant fashion.

The generation of animal models that reproducibly recapitulate characteristic features of PD is necessary for studies to elucidate

* Corresponding author. Department of Neurological Sciences, University of Nebraska Medical Center, Omaha, NE, 68198, USA.
E-mail address: kelly.stauch@unmc.edu (K.L. Stauch).
[1] These authors contributed equally to the manuscript.

https://doi.org/10.1016/j.bbih.2023.100656
Received 14 June 2023; Accepted 15 June 2023
Available online 19 June 2023

mechanisms of disease pathogenesis, enable diagnostic and prognostic biomarker screens, and to develop and test therapeutic strategies. Animal models treated with the neurotoxin methyl-4-phenyl-1,2,3,6-tetrahydropyridine (MPTP) and 6-hydroxydopamine (6-OHDA) have yielded a great wealth of information. Studies using MPTP have been important for understanding nigral DA neuron loss and subsequent striatal adaptations and pointed to the role of mitochondria in PD pathogenesis. However, the pathogenic background of the MPTP model is of a toxic nature rather than a neurodegenerative process as in human PD (Klemann et al., 2016). The intracerebral infusion of 6-OHDA is also of a toxic nature and induces massive destruction of nigrostriatal DA neurons. Studies using 6-OHDA have allowed investigation of motor and biochemical dysfunctions in PD (Grigoryan et al., 1996). While the majority of PD cases are idiopathic, the identification of hereditary forms of PD uncovered gene mutations and variants, such as loss-of-function mutations in *PARK6* and *PARK2*, the genes encoding mitochondrial quality control proteins PTEN-induced putative kinase 1 (Pink1) and the E3 ubiquitin ligase Parkin, which could be harnessed to create animal models (Klein and Westenberger, 2012). In Drosophila, Pink1 mutation results in a reduction in life span and degeneration of muscles and DA neurons, while Parkin mutations led to a defect in their ability to fly and climb (Clark et al., 2006; Park et al., 2006). These behavioral defects were driven by cell death of muscle subsets and DA neuronal degradation (Greene et al., 2003; Whitworth et al., 2005). Unfortunately, mice are resistant to neurodegeneration upon the loss of Pink1 and Parkin (single or double deletion) (Gispert et al., 2009; Goldberg et al., 2003; Kitada et al., 2007, 2009; Von Coelln et al., 2004), while in rats, Pink1 but not Parkin deficiency does lead to motor impairment and nigral DA neuron loss, but without complete penetrance (Creed et al., 2019; Dave et al., 2014; de Haas et al., 2019; DeAngelo et al., 2022; Grant et al., 2015; Kelm-Nelson et al., 2021; Orr et al., 2017; Villeneuve et al., 2016).

Here, we describe the generation and phenotypic characterization of a novel rat model of PD through combined knockout of Pink1 and Parkin. Motor dysfunction, specifically early gait abnormalities and decreased rearing frequency were present in Pink1/Parkin dKO rats. Pink1/Parkin dKO rats exhibited elevated plasma levels of neurofilament light chain and significant loss of tyrosine hydroxylase expression in the SNpc, suggesting DA neuron loss. Glial cell activation was also observed in the SNpc. Pink1/Parkin dKO rats showed elevated plasma and reduced cerebrospinal levels of α-syn as well as the presence of α-syn aggregates in the striatum. Further, the profile of circulating lymphocytes was altered, as elevated $CD3^+CD4^+$ T cells and reduced $CD3^+CD8^+$ T cells in Pink1/Parkin dKO rats were found. This coincided with mitochondrial dysfunction and infiltration of $CD3^+$ T cells in the striatum. These rats reproducibly exhibit PD-relevant abnormalities, particularly in males, enabling studies on PD pathogenesis as well as potential preventative and therapeutic paradigms.

2. Materials and methods

2.1. Generation of Pink1/Parkin double knockout (dKO) rats

The generation and characterization of Pink1 and Parkin single KO rats has been described previously (Dave et al., 2014). The Pink1 and Parkin single KO rats were obtained from SAGE Labs (and now available from Envigo). Pink1/Parkin double knockout (dKO) rats were generated by crossing $Pink1^{-/-}$ rats with $Parkin^{-/-}$ rats to obtain $Pink1^{+/-}$/$Parkin^{\pm}$ rats, which were interbred to obtain $Pink1^{-/-}$/$Parkin^{-/-}$ rats (now available from Envigo). To confirm the deletion of 26 bp in *Park6* (gene encoding Pink1), genotyping was performed using 5′-CCCTGGCTGACT ATCCTGAC-3′ forward and 5′-CCACCACCCACTACCACTTACT-3′ reverse primers. Deletion of 5 bp in *Park2* (gene encoding Parkin) was tested after DNA was amplified using a forward 5′-GGTGTCTTGGCTCAGT GTGA-3′ and reverse 5′-GCCACCCAGAATAGCATCTC-3’. Amplified Polymerase Chain Reaction (PCR) samples were sent to ACGT Inc (Wheeling, IL) for sequencing. Further, a *Park2* deletion primer set was developed in our lab that can be amplified using PCR using Wild Type forward 5′-CCAGTCTCGGAATTGCCTGTCCC-3′ and reverse 5′-TCTGC AGGTGCCGCACTGAAC-3′, and Parkin Deletion forward 5′-AATTTCCC GGTGCTGCAAACAC-3′ and reverse 5′-GTCTGCAGGTGCCGCACTCGG A-3’ (Supplemental Fig. S1). All rats were kept on the Long Evans Hooded (LEH) background. Pink1/Parkin dKO rats were viable and fertile; however, a high death rate of dams during childbirth was observed (approximately 30%). Only male rats were utilized in these experiments, and all rats were weighed at 1, 3, 6, 9, and 12 months. The average body weight of Pink1/Parkin dKO rats was significantly higher than wild-type (WT) controls at 9 and 12 months of age (Supplemental Fig. S2). One 9-month-old WT rat was excluded from the study since it developed an abdominal tumor. Rats were kept in a tempe rature-controlled environment with a 12-h light/dark cycle and free access to rat chow and water. Experiments were conducted in accordance with the National Research Council’s Guide for the Care and Use of Laboratory Animals and the National Institutes of Health requirements, and were approved by the University of Nebraska Medical Center Institutional Animal Care and Use Committee (IACUC). This report adheres to the ARRIVE guidelines.

2.2. Cylinder test

The cylinder test was used to assess rearing frequency and spontaneous forelimb use during rearing. In brief, rats at 1, 3, 6, 9 and 12 months of age were placed in a transparent cylinder with a mirror at a 45° angle placed below the cylinder to facilitate capture of the rearing and forelimb use from beneath the cylinder. Rats were placed in the cylinder for 5 min, and activity was recorded using a Sony HDR-CX210 video camera. The cylinder was cleaned with 70% ethanol between animals. Recordings were analyzed blindly with respect to animal genotype by 3 individuals, and then the number of rears and forepaw touches during rearing from the 3 individuals were averaged for each rat.

2.3. Open field test

The open field test was used to assess rearing frequency for both unsupported and supported rears, as well as response to levodopa treatment. Briefly, rats at 12 months of age were placed in the open field arena consisting of four transparent Plexiglas walls and a white PVC floor. Prior to testing each animal, the entire open field arena was cleaned using 70% ethanol. All open field tests were 5 min in duration, and activity was recorded from the side and above. On day 1, the rats were removed from their home cage and placed in the open field. On day 2, the rats were injected with benserazide (12.5 mg/kg) 30 min prior to levodopa (10 mg/kg) administration. The rats were removed from their home cage and placed in the open field 60 min after levodopa administration. Benserazide and levodopa were both dissolved in saline and injections were intraperitoneal. Recordings were analyzed blindly with respect to animal genotype with the number of unsupported and supported rears during rearing averaged for each rat.

2.4. Gait analysis

A RatWalker system was developed by our group to measure gait in rats (Stauch et al., 2021) based on adaptations to the MouseWalker system developed to measure gait in mice (Mendes et al., 2015). Briefly, the rat home cage was placed at the end of the walker so the rats could walk freely on the walking floor toward their home cage without turning. The rats’ gait was captured from a mirror at 45° angle beneath the walking floor using GoPro Hero6 camera that was set to record 120 frames/second. Videos were then trimmed to include 4 complete strides per rat from each of the 3 trials, converted into a series of images using ImageJ, and uploaded to the MouseWalker software which was written

in MATLAB (Mendes et al., 2015). The software was able to measure different gait parameters including stride velocity, stride length, step cycle, swing duration, stance duration, and swing velocity. Data representing left and right limbs were grouped.

2.5. Immunofluorescence staining and confocal microscopy

Rats were anesthetized with isoflurane and euthanized at 12 months of age by decapitation. Brains were removed and fixed in 4% paraformaldehyde for 24 h at 4 °C. Brains were then rinsed with 1x PBS three times for 10 min prior to cryoprotection using 30% sucrose for 2 days at 4 °C. After cryoprotection, the brains were rinsed with 1x PBS and then embedded in 3% agar for tissue sectioning using a vibrating microtome (Leica Biosystems VT1000S, Buffalo Grove, IL, USA). 50-μm coronal sections were collected on SuperFrost Plus slides (Fisher Scientific) after slicing and stored at −20 °C until staining.

Tissue slides were briefly washed in 1x PBS and blocked/permeabilized for 1 h with a 1x PBS solution containing 5% donkey (Jackson ImmunoResearch Laboratories) and goat serums (Vector Laboratories) and 0.5% Triton X-100 (Sigma-Aldrich). Slides were then incubated overnight at 4 °C with primary antibodies: α-Synuclein Aggregate (Lewy Body) (1:3000, Cat #ab209538, Abcam, Waltham, MA, USA), CD3e (1:150, Cat #MA1-90582, RRID #AB_1956722, ThermoFisher, Waltham, MA, USA), Tyrosine Hydroxylase (TH) (1:2000, Cat #MAB318, Lot #2464515, Millipore, Temecula, CA, USA), α-Synuclein (1:1000, Cat #D37A6, Lot #4179, Cell Signaling Technology, Danvers, MA, USA), GFAP (1:1000, Cat #EPR1034Y, Lot #68428, Abcam), and Iba1 (1:500, Lot #019–19741, FUJIFILM, Chuo, Osaka, Japan). After primary antibody incubation, slides were rigorously washed in 1xPBS and incubated for 2 h at room temperature with secondary antibodies: Alexa Donkey anti-Mouse 647 (1:1000, Cat #A-31571, Invitrogen, Waltham, MA, USA) and Alexa Goat anti-Rabbit 568 (1:1000, Cat #A-11036, Invitrogen). The slides were rinsed and incubated for 10 min with DAPI (5 μg/ml, Cat #D1306, Lot #2328994, Invitrogen) for nuclear counterstain. After a final set of washes, the microscope slides were mounted using Vectashield Plus Antifade Mounting Medium (Cat #H-1900, Vector Laboratories) and placed under coverslips (Fisher Scientific) for them to be imaged using a confocal microscope.

Stained slides were imaged at 4x, 10x, 20x (~25 z-stacks), 40x (~25 z-stacks), and 60x (~12 z-stacks) using a Nikon A1R upright confocal microscope. The images were obtained at 1024x1024 pixel size (1-μm steps for the z-stacks) with 561 and 640 nm lasers.

Analysis was performed in ImageJ (https://imagej.nih.gov/ij/) including: percent area (% area) quantification of 10x images from five different sections, morphology observations, and puncta/cell counts for the corresponding 4x and 10x images. Percent area was obtained by setting a consistent threshold across all images and generating an ROI of interest (substantia nigra pars compacta or striatum) to then measure the signal's area, area fraction (% area), and the mean gray value. These area fractions provided a quantification of the fluorescent signals from the selected area of interest. For counting puncta/cells, the Cell Counter plugin (https://imagej.nih.gov/ij/plugins/cell-counter.html) was used to count each of the objects of interest in a non-biased manner.

2.6. Enzyme-linked immunosorbent assays (ELISAs)

Cerebrospinal fluid (CSF) was collected from the rats at 12 months via the intra-cisterna magna using a ½ inch 25 G needle. Peripheral blood was collected using vacutainer tubes containing K_2EDTA from the rats at 1, 3, 6, 9, and 12 months and plasma was isolated. CSF and plasma were stored at −80 °C. ELISAs for rat α-syn and rat NfL were performed according to manufacturer's recommendations (LS Bio). Standard curves were fit using a sigmoidal, four parameter logistic (4 PL) on GraphPad Prism 9. The CSF samples were diluted 1:5 and assayed in duplicate. The plasma samples were diluted 1:3 and 1:9 and assayed in duplicate. The standard curves for each individual plate were used to transform the absorbance values for that particular plate into protein concentrations (pg/mL) and the two dilutions were then averaged. This way, any variation between plates and sample preparation would be nullified.

2.7. PBMC isolation and hematological profiling

Peripheral blood was collected using vacutainer tubes containing K_2EDTA from the rats at 12 months and PBMCs were isolated. Whole blood was centrifuged at 900×*g* for 20 min at RT to separate erythrocytes, plasma, and the buffy coat. Plasma was collected and stored at −80 °C. The buffy coat was removed, diluted with 1x PBS, and overlayed on Ficoll-Hypaque prior to centrifugation at 400×*g* for 30 min at RT. The PBMC layer was collected, diluted with 1x PBS, and centrifuged at 500×*g* for 7 min at RT. The resulting pellet was lysed with 1x RBC lysis buffer, diluted with 1x PBS, and centrifuged at 400×*g* for 7 min at RT. The PBMC pellet was resuspended in 1x PBS and counted using a Beckman Coulter z1 particle counter. PBMCs were cryopreserved in Fetal Bovine Serum with 10% DMSO and stored in liquid nitrogen. Cells were thawed within 6 weeks of isolation and underwent flow cytometric assessments. Peripheral blood was also collected from the rats at 9 and 12 months of age and processed for blood cell enumeration using the Hemavet 950 FS according to the manufacturer's instructions (Drew Scientific). A significant elevation in the number of platelets was found in the Pink1/Parkin dKO rats at both ages, while the profiles of all other blood elements remained unaltered (Supplementary Fig. S3).

2.8. Flow cytometry

PBMCs were washed and stained with Live/Dead Fixable Blue Dead Cell Stain (L3224, Invitrogen) in PBS. Cells were then washed and blocked with anti-CD32 (Clone D34-485, 1:50) BD Biosciences) to prevent Fc-Mediated non-specific binding. After blocking, cells were stained with antibodies in staining buffer containing PBS, 1% Bovine Serum Albumin (BSA), and 0.1% Sodium Azide at 4 °C for 30 min in the dark. Antibodies used were CD45 (Clone OX-1, 1:100, BV605), CD4 (Clone OX-35, 1:100, V450), CD8 (Clone OX8, 1:100, BUV805), and B220 (Clone HIS24, 1:100, BB700) from BD Biosciences; CD3 (Clone REA223, 1:100, APC) from Miltenyi Biotec, and CD161 (Clone 3.2.3, 1:100, BUV805) from BioLegend. Cells were then washed with staining buffer and fixed in a buffer containing PBS and 4% paraformaldehyde. Flow cytometric compensation was performed using OneComp eBeads and the samples were analyzed using a BD LSRFortessa X50 (BD Biosciences) with laser - filters: 355 nm - 450/50 (Live/Dead), 405 nm - 610/20BP (CD45), 638 nm - 670/30BP (CD3), 405 nm - 427/25BP (CD4), 355 nm - 820/60BP (CD8), 488–525/50BP (CD161), and 488 nm - 710/50BP (B220). Gating strategy, controls, and data provided as **Supplementary File S1**.

2.9. Bioenergetics

Oxygen consumption rates (OCR) and extracellular acidification rates (ECAR) were measured at 37 °C on the Seahorse XFe96 Extracellular Flux Analyzer using 6 technical replicate wells for each independent biological replicate (n = 6 for WT and n = 5 for dKO). PBMCs were plated at 750,000 cells/well in XF assay medium containing 4 mM L-glutamine and 25 mM glucose. Three baseline measurements of OCR and ECAR were recorded prior to sequential injection of oligomycin (O, 3.5 μM, ATP synthase inhibitor), carbonyl cyanide 4-(trifluoromethoxy) phenylhydrazone (FCCP, F, 1 μM, mitochondrial oxidative phosphorylation uncoupler), rotenone (R, 14 μM, complex I inhibitor) and antimycin A (A, 14 μM, complex III inhibitor). For OCR measurements: non-mitochondrial respiration, which corresponds to the average of the three measurement values after injection of rotenone combined with antimycin A, for each well was subtracted from all other values for that well before calculation of the following mitochondrial respiratory

parameters: basal respiration (average of the first three measurement values before the injection of oligomycin); maximal respiration (average of the three measurement values after the injection of FCCP); respiration driving proton leak (average of the three measurement values after the injection of oligomycin); respiration driving ATP synthesis (basal respiration minus respiration driving proton leak); and spare respiratory capacity (maximal respiration minus basal respiration). For ECAR measurements, the glycolytic parameters: basal glycolysis (the average of the first three measurement values before the injection of oligomycin), maximal glycolysis (the average of the three measurement values after the injection of oligomycin), and glycolytic reserve capacity (maximal glycolysis minus basal glycolysis) were calculated. For comparisons across assay plates using independent PBMC isolations for each plate, absolute rates of OCR and ECAR were converted to relative percent response from baseline (third measurement before oligomycin injection). The Seahorse Wave Controller Software 2.6 package was used for data collection.

2.10. Statistical analysis

Grubb's test ($\alpha = 0.05$) identified outliers (GraphPad Software 9). To compare the means between two groups, statistical significance was

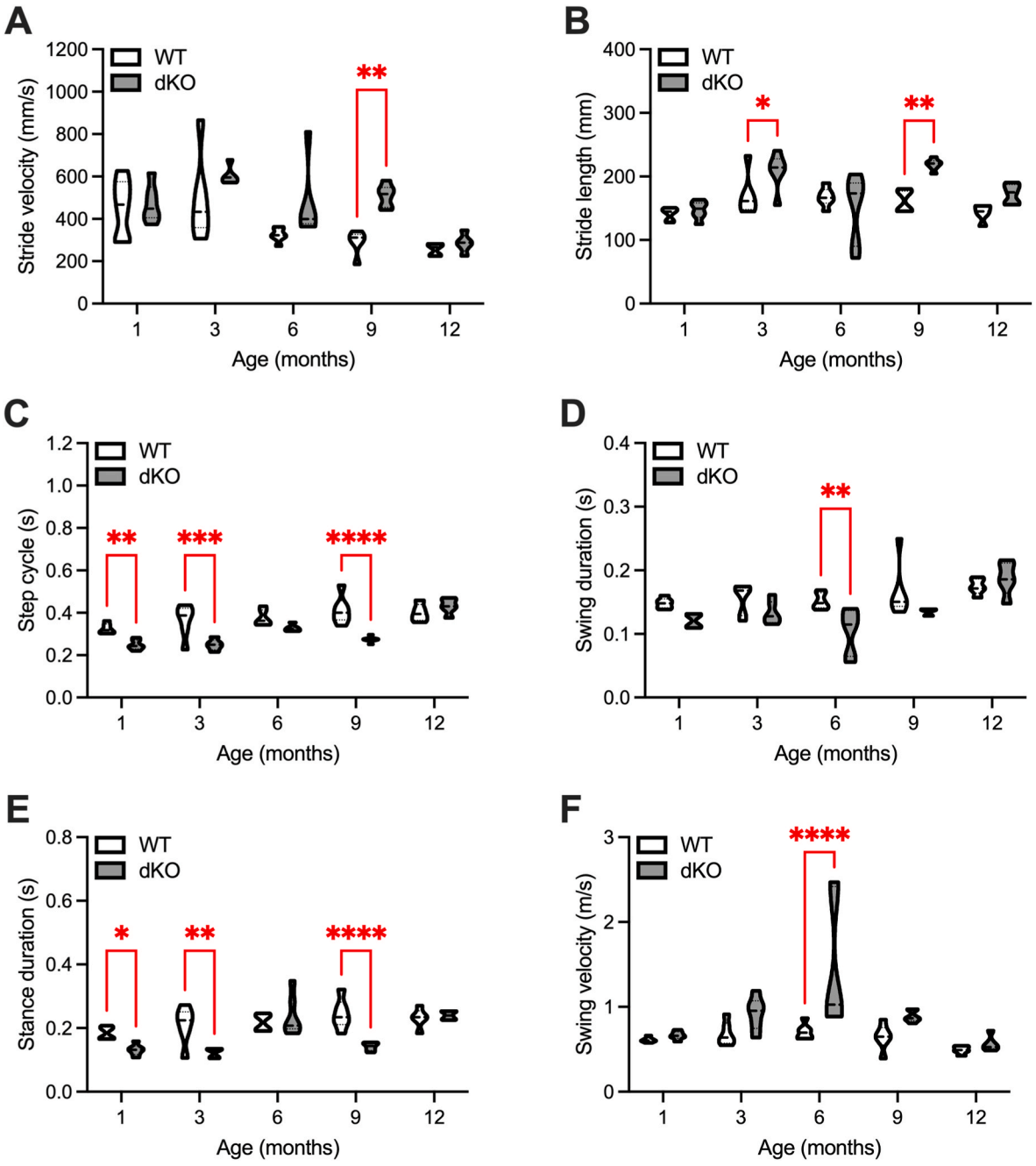

Fig. 1. Effects of double deletion of Pink1 and Parkin on gait via conventional analysis. Graphs demonstrating: (A) the time in seconds between two consecutive initial walkway contacts of the same paw (step cycle), which consists of the (B) duration in seconds of contact of a paw with the walkway (stance phase) and (C) the duration in seconds of no contact for a paw with the walkway (swing phase). LF, left front; RF, right front; LH, left hind; RH, right hind. Data shown as truncated violin plots with median and quartiles indicated by black horizontal lines. Significant in dKO compared to WT (n = 4–6 per group; $p < 0.05$*, 0.01**, 0.001***, 0.0001****) using two-way ANOVA followed by Holm-Sidak multiple comparisons test. (For interpretation of the references to colour in this figure legend, the reader is referred to the Web version of this article.)

assessed by unpaired parametric two-tailed *t*-test (GraphPad Software 9). For comparing the means among three or more groups, statistical significance was assessed by two-way ANOVA and Holm-Sidak's multiple comparisons test (GraphPad Software 9). The relationship between each gait parameter and velocity was compared using nonlinear least squares regression (second order polynomial (quadratic)) and extra sum-of-squares F test (GraphPad Software 9).

3. Results

3.1. Pink1/parkin dKO rats show gait abnormalities

Gait disturbances are a defining feature of PD occurring early during disease course and include decreased arm swing, slower walking speed, and shorter steps (Zanardi et al., 2021). We previously reported gait abnormalities in Pink1/Parkin dKO rats at an early age, 2 months (Stauch et al., 2021). Here, to evaluate the age-related progression of the gait changes, we quantitatively examined the walking behavior in freely

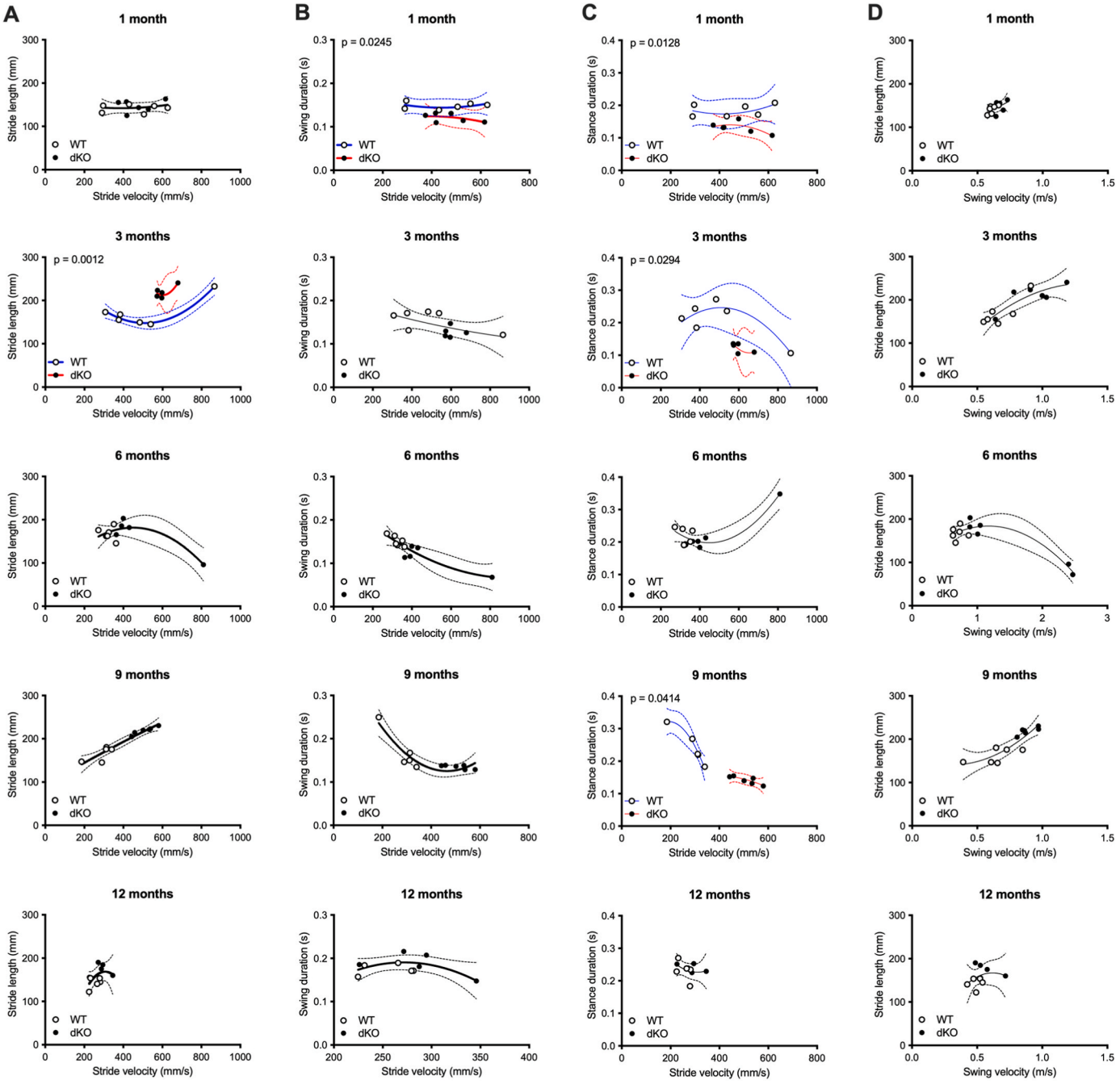

Fig. 2. Regression analysis to reveal gait quality changes in dKO rats. Visualization of gait parameters plotted as a function of speed (stride and swing velocity). Relationships of (A) stride length, (B) swing duration, and (C) stance duration as a function of stride velocity. (D) Relationship of stride length as a function of swing velocity. Each of the parameters behaves differently as a function of velocity with aging, as illustrated by best fit non-linear regression curves (solid lines) and 95% confidence bands (dashed lines). The fit of one curve to both data sets was compared with the fit of individual curves fit to each dataset. Gait parameters with significant differences between WT and dKO rats (Extra sum-of-squares F test) are highlighted in blue (WT) and red (dKO). (For interpretation of the references to colour in this figure legend, the reader is referred to the Web version of this article.)

walking Pink1/Parkin dKO and WT rats at 1, 3, 6, 9, and 12 months of age using an optical touch sensor based on frustrated total internal reflection (FTIR). It is important to note that the Pink1/Parkin dKO rats experience temporary hindlimb dragging, which was previously reported in male Pink1 single KO (sKO) rats (Dave et al., 2014). In contrast to Pink1 sKO rats where approximately 30% of males exhibit hindlimb dragging, we find that 100% of male Pink1/Parkin dKO rats exhibited this phenotype by 6 months of age. The earliest age of onset observed was 4 months of age. The duration of this hindlimb dragging varies with resolution within 4–8 weeks after onset. As such, at 6 months of age, the gait analysis was complicated by the fact that the Pink1/Parkin dKO rats exhibit hind-limb dragging, and as such animals unable to swing their hind limbs were excluded.

Spatial (stride length) and temporal (stance and swing duration, swing velocity) gait measurements that are known to be speed dependent were obtained. Stride velocity was significantly increased in dKO rats compared to WT rats at 9 months of age only (no significant changes were found at 1, 3, 6, and 12 months, Fig. 1A). Conventional analysis of the gait data independent of speed revealed several differences between WT and dKO rats. The stride length was significantly increased at 3 and 9 months for dKO rats (Fig. 1B). Step cycle is the time between two consecutive initial contacts of the same paw with the walkway floor. When we examined the duration of the step cycle each age, significant differences were observed in the dKO rats compared to WT rats, in which a decrease in the average duration of step cycle was observed at 1, 3, and 9 months of age (Fig. 1C). The step cycle is composed of two stages, the stance phase, which is the duration of contact of a paw with the walkway floor, and the swing phase, which is the duration of no contact of a paw with the floor. When we examined the swing duration, we found significant reductions for dKO rats at 6 months (Fig. 1D). We found significant reductions for dKO rats in the stance duration at 1, 3, and 9 months (Fig. 1E). The swing velocity was unaltered, except at 6 months where it was increased for dKO rats (Fig. 1F).

Analyzing gait data sets as a function of walking speed (stride velocity) allows one to assess whether a change in a gait parameter reflects a change in velocity only or a change in gait quality or signature. Such analysis can be performed by testing whether best-fit regression curves representing the datasets from the animals with different genetic backgrounds are shared (Broom et al., 2017). For each age, we compared the fit of individual curves to each dataset to the fit of one curve to both data sets combined by an F-test. The stride length changes we observed for dKO rats at 3 months (Fig. 1B) are due to a change in gait quality or signature rather than a change in velocity, since we found significant differences in the stride length as a function of stride velocity regression curves (Fig. 2A). In contrast, the stride length changes observed at 9 months (Fig. 1B) appear to be velocity-dependent since the comparison of curves did not reveal significant differences (Fig. 2A). Regression analysis of swing duration data in a velocity-dependent manner revealed significant differences at 1 month (Fig. 2B) although decreased swing duration by conventional analysis did not reach significance at this age (Fig. 1D) pointing to changes in gait signature. Of note, the comparison of curves for swing duration as a function of stride velocity at 6 months was not significant (Fig. 2B) so the reduced swing duration at 6 months (Fig. 1D) is velocity dependent. Stance duration decreases observed at 1, 3, and, 9 months (Fig. 1E) are due to altered gait quality as revealed by the significant regression analysis (Fig. 2C). A comparison of curves did not reveal significant differences in stride length as a function of swing velocity at any age (Fig. 2D). This reveals that the changes in stride length are dependent on swing velocity.

Summarizing, these data show that double deletion of Pink1 and Parkin affects both spatial and temporal aspects of gait, including changes in gait quality/signatures, and that these alterations are dependent on the age examined.

3.2. Reduced rearing frequency and tremorigenesis in Pink1/Parkin dKO rats

To investigate whether the combined deficiency of Pink1 and Parkin leads to functional deficits in limb activity and/or locomotor asymmetry, the cylinder test was used to measure rearing frequency and spontaneous forelimb use in the rats at 1, 3, 6, 9, and 12 months of age. While no significant alterations in rearing frequency were uncovered at 1 and 3 months of age, at 6, 9, and 12 months of age the Pink1/Parkin dKO rats exhibited a significant reduction in the number of rears compared to age-matched WT controls (Fig. 3A, Supplementary Videos 1 and 2). While both the WT and Pink1/Parkin dKO rats used the right and left paw indifferently at 6 and 12 months of age (Supplementary Fig. S4), Pink1/Parkin dKO rats showed a reduced number of paw touches using both simultaneously (Fig. 3B) as well as the left (Fig. 3C) and right (Fig. 3D) paws separately as compared to WT controls, which corresponds to the decreased rearing frequency. We did uncover preferential use of the right over left paw in WT rats at 3 months of age (Supplementary Fig. S4), which was unexpected. This finding highlights the importance of assessing the number of paw touches for each paw before brain injury to establish a baseline when using injury and lesion models, including the 6-OHDA and MPTP models of PD.

To confirm the cylinder test results, rearing frequency at 12 months of age was also evaluated in an open field and consistent with the cylinder test findings Pink1/Parkin dKO rats showed reduced rearing frequency (Fig. 4A, Supplementary Videos 3 and 4). Specifically, we found that the Pink1/Parkin dKO rats exhibited lower frequency of unsupported rears. To evaluate the motor response to levodopa in the Pink1/Parkin rats, rearing frequency was measured before and after levodopa treatment. As seen in Fig. 4B (Supplementary Video 5), treatment with levodopa resulted in a shift in rearing frequency characterized by a decrease in the number of supported rears and an increase in the number of unsupported rears.

In addition to the hindlimb dragging phenotype, several other qualitative visual observations were made, including observing tremors in the dKO rats while at rest, especially prominent in the forelimbs as well as the lower trunk and flank (**Supplementary Video 4**). Tremor is one of the most visible features of PD, and the typical PD tremor occurs at rest and usually begins in a limb, often in hands or fingers (Heusinkveld et al., 2018). Further, the dKO rats exhibit abnormal movements of the mouth and tongue (**Supplementary Video 4**) reminiscent of lingual dyskinesia or lingual protrusion dystonia, which are described in PD patients (Maiola et al., 2016; Sheehy et al., 2008). While rats can't vomit, they can regurgitate, and the dKO rats appear to occasionally undergo retching movements (**Supplementary Video 4**), suggesting they may be experiencing gastroparesis, another symptom in PD. These behaviors appeared at least partially ameliorated by levodopa treatment as the observed frequency and severity was reduced (**Supplementary Video 5**).

Supplementary video related to this article can be found at https://doi.org/10.1016/j.bbih.2023.100656

3.3. Elevated NfL levels in plasma and loss of tyrosine hydroxylase staining in the SNpc of Pink1/Parkin dKO rats

PD is characterized by the progressive loss of DA neurons in the SNpc, and previous studies have reported DA neurodegeneration in Pink1 sKO rats but not in Parkin sKO rats (Dave et al., 2014; DeAngelo et al., 2022; Villeneuve et al., 2016). To determine if combined deficiency of Pink1 and Parkin results in DA neuron loss in the SNpc, brains from 12-month-old WT and Pink1/Parkin dKO rats were immunostained for tyrosine hydroxylase (TH). TH is the rate-limiting enzyme that converts tyrosine to L-DOPA (L-3,4-dihydroxyphenylalanine), a precursor to dopamine and thus a marker of DA neurons. In Pink1/Parkin dKO rats the percent positive area of staining for TH showed significant reductions compared to WT rats (Fig. 5A and B). The TH positive neuron

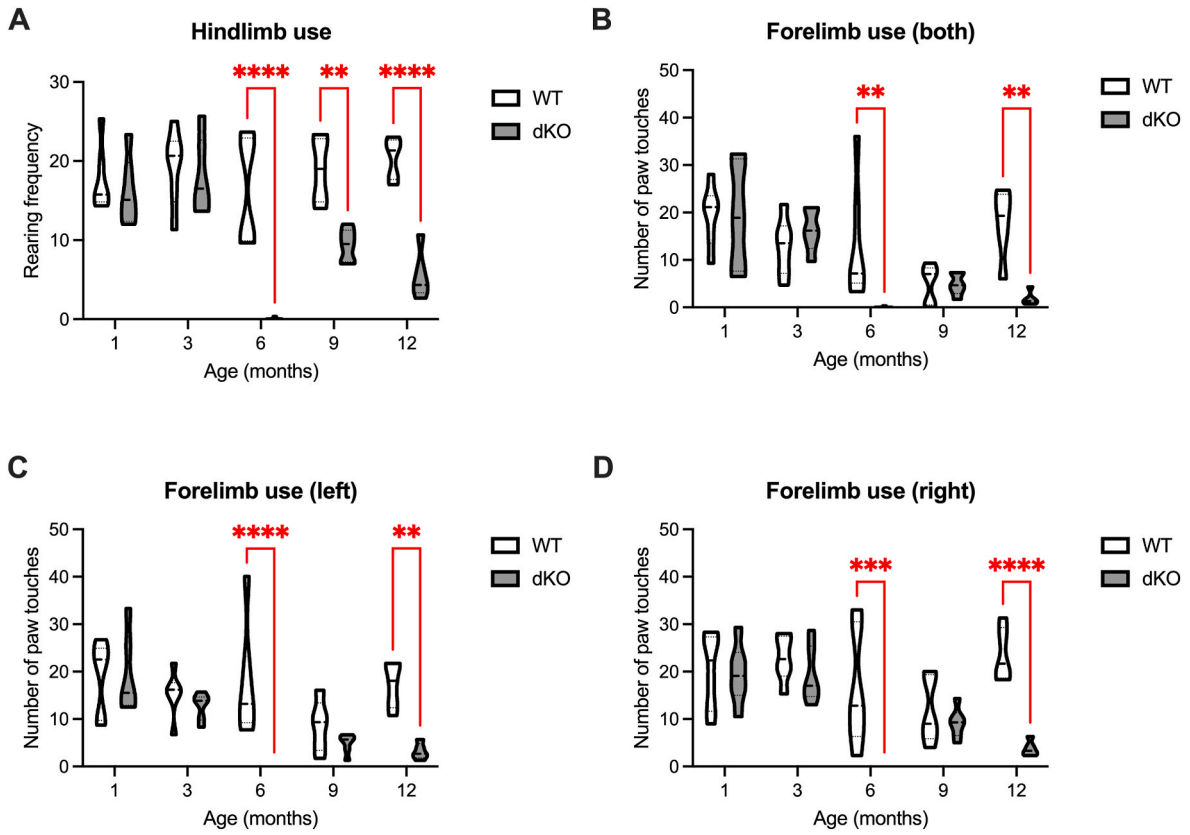

Fig. 3. Cylinder test reveals reduced rearing frequency in dKO rats at 6, 9, and 12 months. The cylinder test was used to assess hindlimb and forelimb use in WT and dKO rats at 1, 3, 6, 9, and 12 months of age. Truncated violin plots with median and quartiles indicated by black horizontal lines. Significant in dKO compared to WT (n = 5–6 per group; p < 0.01**, 0.001***, 0.0001****) using two-way ANOVA and Holm-Sidak multiple comparisons test.

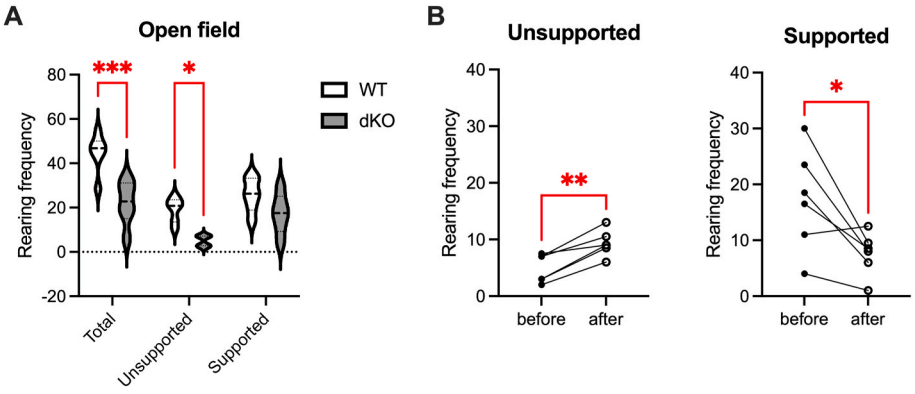

Fig. 4. Open field rearing uncovers impaired unsupported rearing in dKO rats at 12 months that is responsive to levodopa. The open field arena was used to assess unsupported and supported rearing in WT and dKO rats at 12 months of age. (A) Quantification of total, unsupported, and supported rears in WT and dKO rats. Truncated violin plots with median and quartiles indicated by black horizontal lines. Significant in dKO compared to WT (n = 6 per group; p < 0.05*, 0.001***) using two-way ANOVA and Holm-Sidak multiple comparisons test. (B) Quantification of unsupported and supported rears in dKO rats before and after levodopa treatment. Lines connect the data points for the same rat before and after levodopa. Significant after compared to before levodopa (n = 6 per group; p < 0.05*, 0.01**) using unpaired two-tailed t-test.

population appeared relatively healthy in the WT group, unlike in the Pink1/Parkin dKO brains, in which most of the cell bodies were completely absent with some remaining projections across the pars compacta towards the pars reticulata region. Of note, the ventral tegmental area was spared in the Pink1/Parkin dKO rats and exhibited TH staining comparable to WT rats. Neurofilament light chain (NfL), a marker of neuronal degeneration, is elevated in the blood of many patients with neurological and neurodegenerative diseases, including PD (Hansson et al., 2017; Lin et al., 2018; Pilotto et al., 2021a, 2021b). In fact, blood NfL is among the most promising candidate biomarkers of neuroaxonal injury and has been proposed as a blood-based biomarker of neurodegeneration in PD (Backstrom et al., 2020; Hansson et al., 2017). Thus, we measured plasma levels of NfL in the WT and Pink1/-Parkin dKO rats. While unchanged at 1 month, we found significantly increased plasma levels of NfL in the Pink1/Parkin dKO rats at 3, 6, 9, and 12 months of age (Fig. 5C). Taken together, these findings show that elevated plasma NfL levels coincide with reduced TH staining in the SNpc of 12-month-old Pink1/Parkin dKO rats, suggesting loss of DA neurons in the SNpc.

3.4. *Glial morphology changes indicative of activation in the SNpc of Pink1/Parkin dKO rats*

In PD, the loss of DA neurons in the SNpc is associated with a glial response, composed mainly of activated microglia and, to a lesser extent, of reactive astrocytes (Kline et al., 2021). Thus, we performed immunofluorescent staining in the SNpc for Iba1 and GFAP to assess the presence and morphology of microglia and astrocytes, respectively. As

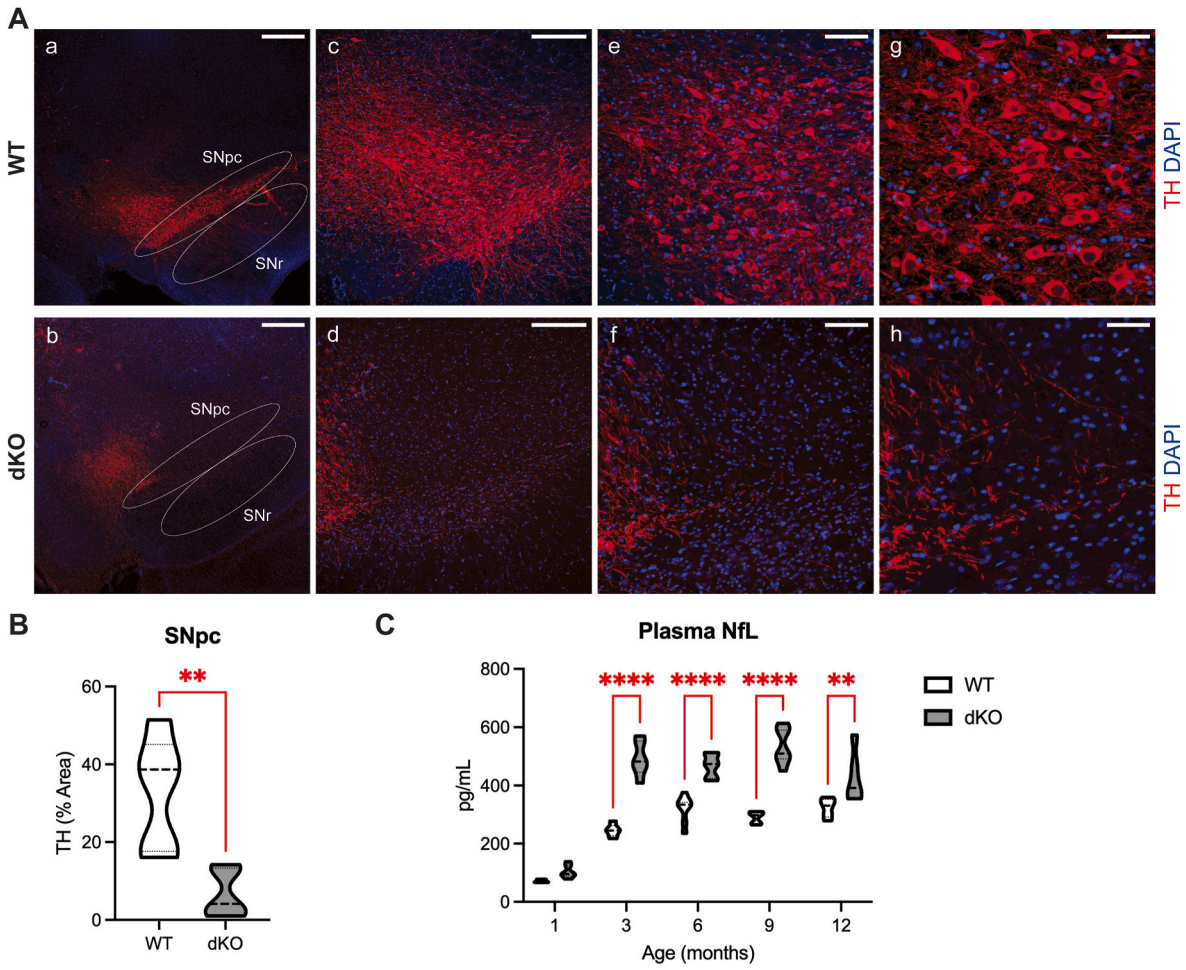

Fig. 5. Loss of TH staining in the SNpc of dKO rats at 12 months. (A) Z-stack maximal projection of a representative TH labeling merged with DAPI on 12-month-old (a, c, e, g) WT and (b, d, f, h) dKO SNpc. Objective/scale bar: (a, b) 4x/500 μm, (c, d) 10x/250 μm, (e, f) 20x/100 μm, (g, h) 40x-oil/50 μm. TH in red, DAPI in blue. White outlines highlighting the SNpc and SNr. (B) Quantification of TH positive staining (% area). Significant in dKO compared to WT ($n = 5$ per group; $p < 0.01$**) using unpaired two-tailed *t*-test. (C) ELISA quantification of NfL in plasma from WT and dKO rats at 1, 3, 6, 9, and 12 months. Significant in dKO compared to WT ($n = 5$–7 per group; $p < 0.01$**, 0.0001****) using two-way ANOVA followed by Holm-Sidak multiple comparisons test. (For interpretation of the references to colour in this figure legend, the reader is referred to the Web version of this article.)

seen in Fig. 6A, the morphology of the microglial cells observed within the SNpc of the Pink1/Parkin dKO rats at 12 months of age exhibited an amoeboid shape, whereas those in the WT rats had normal branching. The retraction of microglial branches towards the circumference of the cell is thought to be correlated with glial activation. Similarly, the astrocytes in the SNpc of the Pink1/Parkin dKO rats appeared swollen with little to no branching reminiscent of gemistocytic reactive astrocytes, whereas the astrocytes in the SNpc of the WT rats maintained their ramified morphology (Fig. 6B). Taken together, these findings reveal glial morphology changes indicative of activation coincide with reduced TH staining in the SNpc of the Pink1/Parkin dKO rats suggesting gliosis likely contributes to pathogenesis in this rat model.

3.5. α-Syn aggregation in the striatum of Pink1/Parkin dKO rats

In addition to loss of DA neurons in the SNpc and the presence of gliosis, the major neuropathological finding in postmortem brains of PD patients is the presence of Lewy bodies (Srinivasan et al., 2021), which are intracytoplasmic inclusions of protein aggregates whose primary component is α-syn. Immunofluorescent staining in the SNpc of the Pink1/Parkin dKO rats at 12 months of age revealed no major changes in α-syn expression; although the pattern of staining appears more diffuse (Supplementary Fig. S5). However, α-syn normally localizes predominantly to presynaptic terminals and α-syn aggregation at the synapse is an early event in PD and is associated with impaired striatal synaptic function (Srinivasan et al., 2021). Thus, we performed immunofluorescent staining for α-syn in the striatum at 12 months of age. As seen in Fig. 7, in the striatum of the Pink1/Parkin dKO rats, α-syn appeared aggregated as puncta and were absent in the WT rat striatum (Fig. 7A). To confirm that the observed α-syn puncta were in fact aggregates, a conformation-specific antibody for α-syn aggregates was used for immunofluorescent staining in the striatum. Indeed, α-syn aggregates were observed in the striatum of the Pink1/Parkin dKO rats but not in the WT rats (Fig. 7B). Measuring α-syn levels in biofluids might be a potential biomarker for PD diagnosis (Chang et al., 2019; Lin et al., 2017); therefore, we used ELISAs to detect α-syn in the cerebrospinal fluid (CSF) and plasma from the rats. The CSF α-syn concentration was significantly decreased in Pink1/Parkin dKO rats compared to WT rats at 12 months of age (Fig. 7C). Conversely, we found overall increased levels of plasma α-syn in the Pink1/Parkin dKO rats compared to age-matched WT rats, with the changes reaching significance at 1, 6, 9, and 12 months of age (Fig. 7D).

3.6. Altered circulating lymphocytes and T cell infiltration into the brain of Pink1/Parkin dKO rats

Literature suggests α-syn might activate T cells in the periphery and that T cell infiltration into the brain might contribute to PD pathogenesis

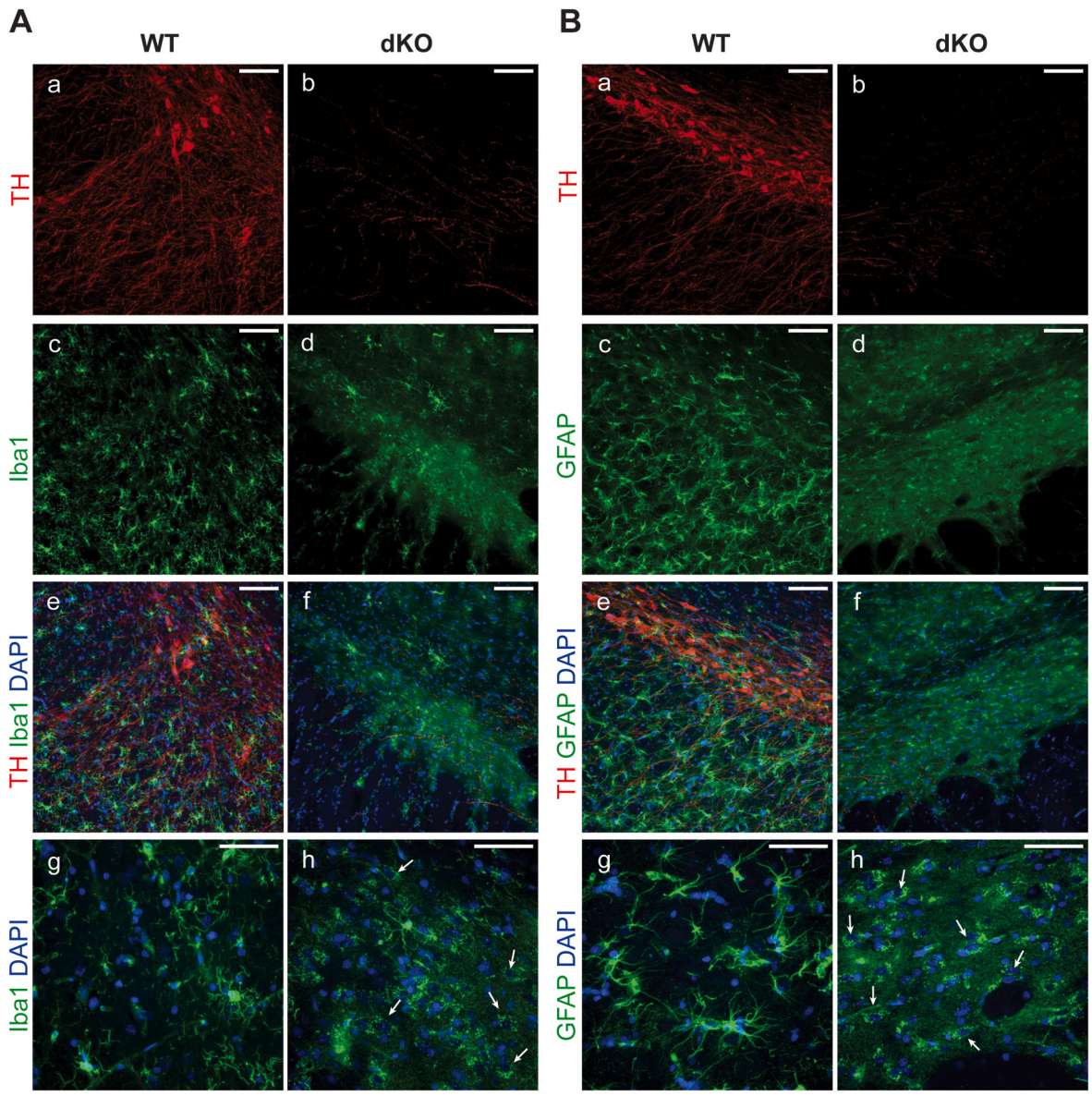

Fig. 6. Gliosis in the SNpc of dKO rats at 12 months. (A) Z-stack maximal projection of a representative (a, b) TH labeling, (c, d) Iba1 labeling, (e, f) TH and Iba1 labeling merged with DAPI, and (g, h) Iba1 labeling merged with DAPI on 12-month-old on 12-month-old (a, c, e, g) WT and (b, d, f, h) dKO SNpc. Objective/scale bar: (a–f) 20x/100 μm, (g, h) 60x-oil/50 μm. TH in red, Iba1 in green, DAPI in blue. (B) Z-stack maximal projection of a representative (a, b) TH labeling, (c, d) GFAP labeling, (e, f) TH and GFAP labeling merged with DAPI, and (g, h) GFAP labeling merged with DAPI on 12-month-old on 12-month-old (a, c, e, g) WT and (b, d, f, h) dKO SNpc. Objective/scale bar: (a–f) 20x/100 μm, (g, h) 60x-oil/50 μm. TH in red, GFAP in green, DAPI in blue. (For interpretation of the references to colour in this figure legend, the reader is referred to the Web version of this article.)

(Brochard et al., 2009; Lindestam Arlehamn et al., 2020; Sulzer et al., 2017). Since we found elevated plasma α-syn levels, we next employed a validated flow cytometric panel (Barnett-Vanes et al., 2016) to characterize the major leukocyte subsets circulating in the periphery using PBMCs from WT and Pink1/Parkin dKO rats at 12 months of age. Using antibodies targeted against a multitude of surface antigens our gating strategy first removed debris and dead cells (LIVE-DEAD stain), cell clumps (FSC-H and FSC-W; exclude doublets and clustered cells), or $CD45^{-}$cells (excludes erythrocytes and plasma cells). This resulted in a population of live leukocytes which were then sequentially separated, first for T lymphocytes by CD3 which were further delineated by CD4 and CD8, and then NK cells were identified by CD161 and B cells by CD45R. Changes in the circulating leukocytes, specifically increased numbers of $CD3^{+}$ $CD4^{+}$ T cells and decreased numbers of $CD3^{+}$ $CD8^{+}$ T cells were found in Pink1/Parkin dKO rats compared to age-matched WT controls (Fig. 8). Further, immunofluorescence staining for CD3 in the striatum revealed increased numbers of $CD3^{+}$ T cells in the Pink1/Parkin dKO rats (Fig. 9). These results indicate that T cells infiltrated into the brain at a time that coincides with the presence of α-syn pathology in the striatum.

3.7. *Impaired mitochondrial respiration in PBMCs from Pink1/Parkin dKO rats*

Since Pink1 and Parkin function together to modulate mitochondrial quality control we used the Seahorse XF analyzer metabolic assay platform to simultaneously assess mitochondrial (OCR, oxygen consumption rate) and glycolytic (ECAR, extracellular acidification rate) function in PBMCs isolated from the 12-month-old WT and dKO rats. As shown in Fig. 10, PBMCs from the dKO rats exhibit impaired maximal mitochondrial function (Fig. 10A) in the absence of changes in glycolysis (Fig. 10B). Fig. 10C shows the OCR versus ECAR showing PBMCs from

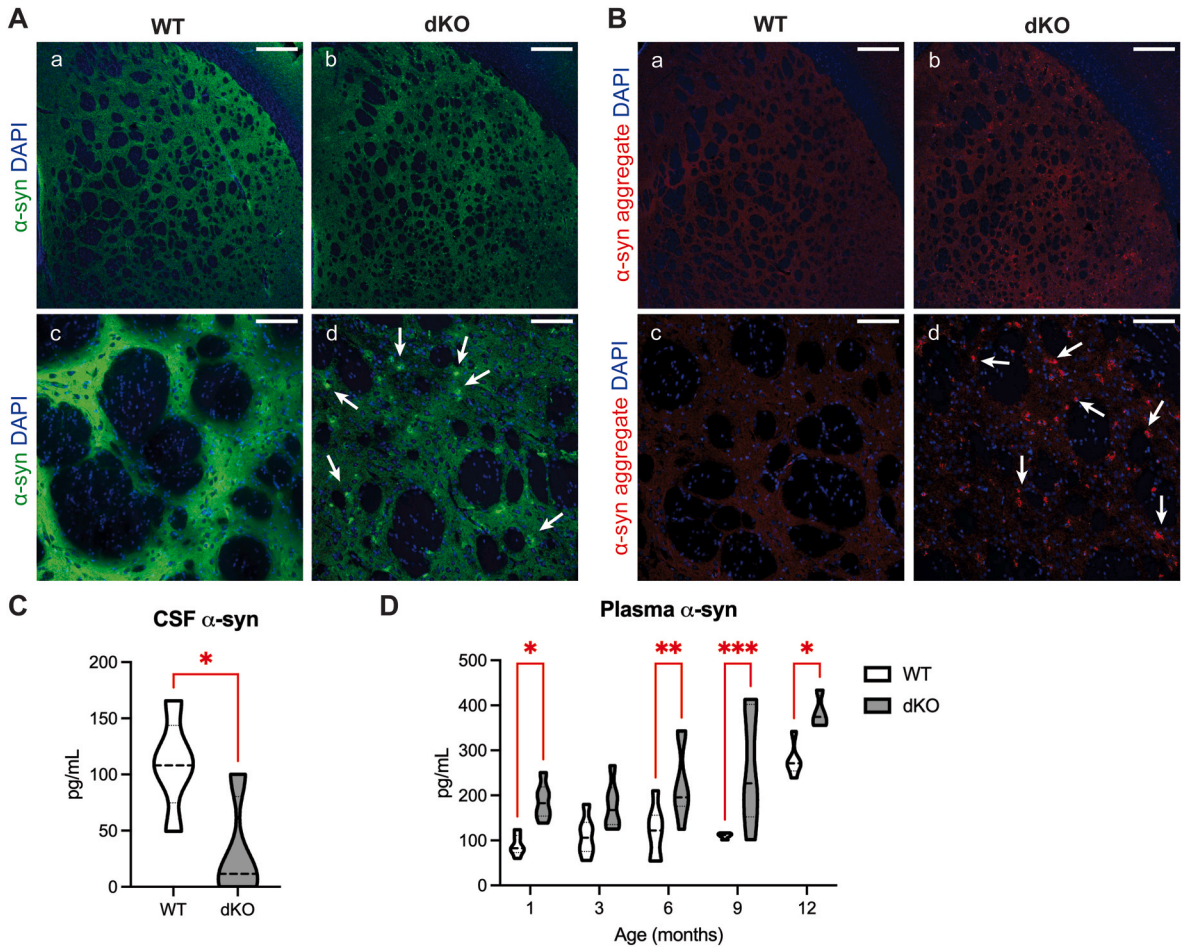

Fig. 7. Aggregated α-syn in the striatum of dKO rats at 12 months. (A) Z-stack maximal projection of a representative α-syn labeling merged with DAPI on 12-month-old (a, c) WT and (b, d) dKO striatum. Objective/scale bar: (a, b) 4x/500 μm, (c, d) 20x/100 μm. α-syn in green, DAPI in blue. (B) Z-stack maximal projection of a representative α-syn aggregate labeling merged with DAPI on 12-month-old (a, c) WT and (b, d) dKO striatum. Objective/scale bar: (a, b) 4x/500 μm, (c, d) 20x/100 μm. α-syn aggregate in red, DAPI in blue. (C) ELISA quantification of α-syn in CSF from WT and dKO rats at 12 months. Significant in dKO compared to WT ($n = 4$–5 per group; $p < 0.05$) using unpaired two-tailed *t*-test. (D) ELISA quantification of α-syn in plasma from WT and dKO rats at 1, 3, 6, 9, and 12 months. Significant in dKO compared to WT ($n = 4$–7 per group; $p < 0.05$*, 0.01**, 0.001***) using two-way ANOVA followed by Holm-Sidak multiple comparisons test. (For interpretation of the references to colour in this figure legend, the reader is referred to the Web version of this article.)

dKO rats have a low OCR and a low ECAR as compared to PBMCs from WT rats, suggesting overall lower metabolic function due to combined loss of Pink1/Parkin.

4. Discussion

In this current study, the Pink1/Parkin dKO rat model was generated and characterized, with the finding of a reproducible mammalian model of PD which will enable mechanistic studies to understand the combined loss-of-function of Pink1 and Parkin. The Pink1/Parkin pathway(s) appear key in PD pathogenesis as well as prevention/treatment paradigms. Pink1 and Parkin are both proteins involved in mitochondrial quality control (Pickles et al., 2018), and when they carry loss-of-function mutations lead to familial forms of PD. Pink1 and Parkin mutation incidence in patients are higher in early-onset PD (<40 years old); however, the pathological features of Pink1 and Parkin are different. Mutation in Parkin induces less severe motor abnormalities and fewer motor complications in response to DA replacement with levodopa, while mutation in Pink1 has a high rate of medication-induced dystonia and development of other non-motor symptoms such as dementia (Lesage et al., 2020). Upon screening for Pink1 mutations in 175 parkinsonism patients with parkin mutations, two sibling pairs and one sporadic patient were found to be carrying both Pink1 and Parkin mutations (Funayama et al., 2008). Thus, the presence of digenic forms of PD highlights the importance of understanding the effects of combined loss-of-function of Pink1 and other PD genes, including Parkin.

To elucidate the pathophysiological changes associated with loss-of-function mutations in Pink1 and Parkin, several different mammalian animal model KOs have been generated and characterized. While the mouse KO model of Pink1 displayed some motor abnormalities, those deficits were mild and there was no sign of DA neuronal loss in the SNpc or DA loss in the striatum (Kitada et al., 2007). Even though Parkin mutation is the most common autosomal recessive form of PD in humans, neither mouse nor rat Parkin KO models showed substantial abnormalities; although a slight impairment in DA release was found in mice (Itier et al., 2003; Kitada et al., 2007). The Pink1 KO rat was one of the first mammalian genetic models to show significant PD-like changes (Dave et al., 2014). These two KO rat models showed motor impairments and DA neuron loss in the SNpc (Dave et al., 2014; DeAngelo et al., 2022; Villeneuve et al., 2016). Further, Pink1 KO rats exhibited abnormalities in basal and evoked DA (Creed et al., 2019). Of note, while male Pink1 KO rats exhibit hind-limb dragging, female Pink1 KO rats do not, and only approximately 30% of the male Pink1 KO rats appear to be affected suggesting incomplete penetrance, which is supported by contradictory findings showing the presence (Dave et al., 2014; DeAngelo et al., 2022;

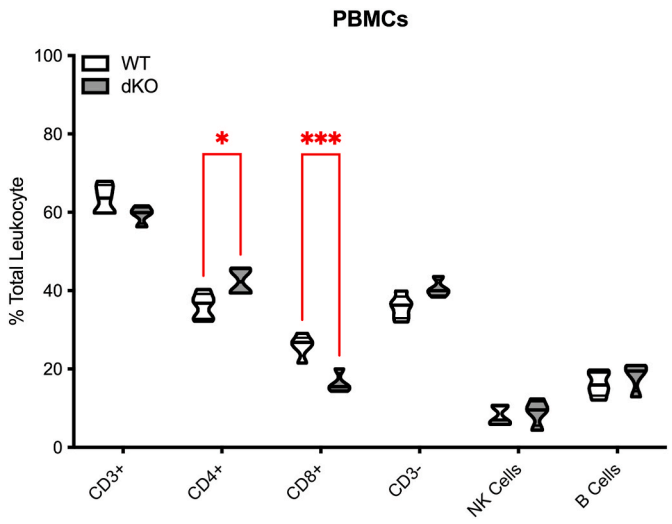

Fig. 8. Altered levels of circulating lymphocytes in dKO rats at 12 months. PBMCs were isolated from 12-month-old WT and dKO rats and processed for flow cytometric analysis. Data shown as truncated violin plots with median and quartiles indicated by black horizontal lines. Significant in dKO compared to WT ($n = 4$–5 per group; $p < 0.05$*, 0.001***) using two-way ANOVA followed by Holm-Sidak multiple comparisons test.

Villeneuve et al., 2016) versus absence (de Haas et al., 2019; Grant et al., 2015; Orr et al., 2017) of significant loss of DA neurons in the SNpc. Incomplete phenotype penetrance can complicate mechanistic studies; however as discussed previously (Kelm-Nelson et al., 2021) Pink1 KO rats indeed mimic the human symptomatology showing motor as well as non-motor and non-classical motor abnormalities and as such are a useful model to study PD.

To assess motor function in the Pink1/Parkin dKO rats, three motor behavior tests were performed: gait analysis, the cylinder test, and open field rearing. To quantitatively assess gait in the freely-walking rats, we used an optical touch sensor based on frustrated total internal reflection (fTIR), which records and tracks the footprints of rodents as they move on a walkway. Using this approach we previously described the walking behavior of WT rats and uncovered gait abnormalities in the dKO rats at 2 months of age (Stauch et al., 2021). We uncovered gait abnormalities in the dKO rats as early as 1 month of age that persisted as they aged to 9 months. Swing velocity, stride velocity and length were increased, while step cycle, swing and stance duration were decreased. Of these, swing duration (at 1 month), stride length (at 3 months), and stance duration (at 1, 3, and 9 months) changes in the dKO rats are due to a change in gait quality or signature rather than a change in velocity. At 12 months of age no significant gait alterations were found in the dKO rats versus the WT rats; however, this could be due to age-related changes in the walking style of the WT rats. Reduced walking speed is a hallmark of functional decline in aging across species, and the slowing of gait during aging combined with the speed dependence of gait metrics imposes challenges when assessing gait signatures in aging animals (Broom et al., 2021). Our findings reveal that the dKO rats have a shorter step cycle and take quicker steps. Individuals with PD walk slower than healthy controls through a largely reduced stride length despite showing higher cadence, and reduced walking speeds denote a compensation strategy to avoid fallings in PD patients (Zanardi et al., 2021).

The cylinder test revealed reduced rearing frequency in Pink1/Parkin dKO rats at 6 months that persisted at 9 and 12 months of age. Previously, a reduction in rearing frequency was reported starting at 4 months in Pink1 KO (but not Parkin KO) rats (Dave et al., 2014). The

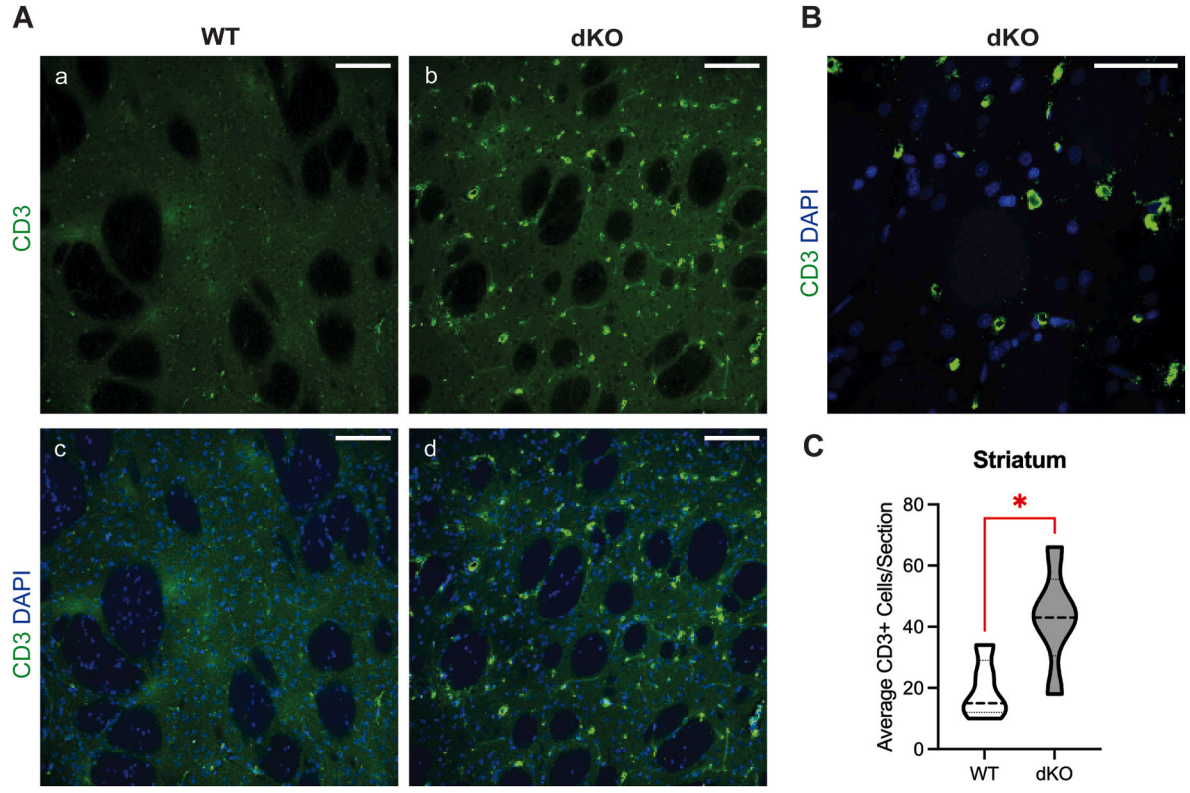

Fig. 9. Increased occurrence of $CD3^+$ T cells in the striatum of dKO rats at 12 months. (A) Z-stack maximal projection of a representative (a, b) CD3 labeling and (c, d) CD3 labeling merged with DAPI on 12-month-old on 12-month-old (a, c, e, g) WT and (b, d, f, h) dKO striatum. Objective/scale bar: (a–d) 20x/100 μm. CD3 in green, DAPI in blue. (B) Z-stack maximal projection of a representative CD3 labeling merged with DAPI on 12-month-old dKO striatum. Objective/scale bar: 60x-oil/50 μm. CD3 in green, DAPI in blue. (C) Quantification of CD3 positive staining (number of cells/section). Significant in dKO compared to WT ($n = 5$ per group; $p < 0.05$*) using unpaired two-tailed *t*-test. (For interpretation of the references to colour in this figure legend, the reader is referred to the Web version of this article.)

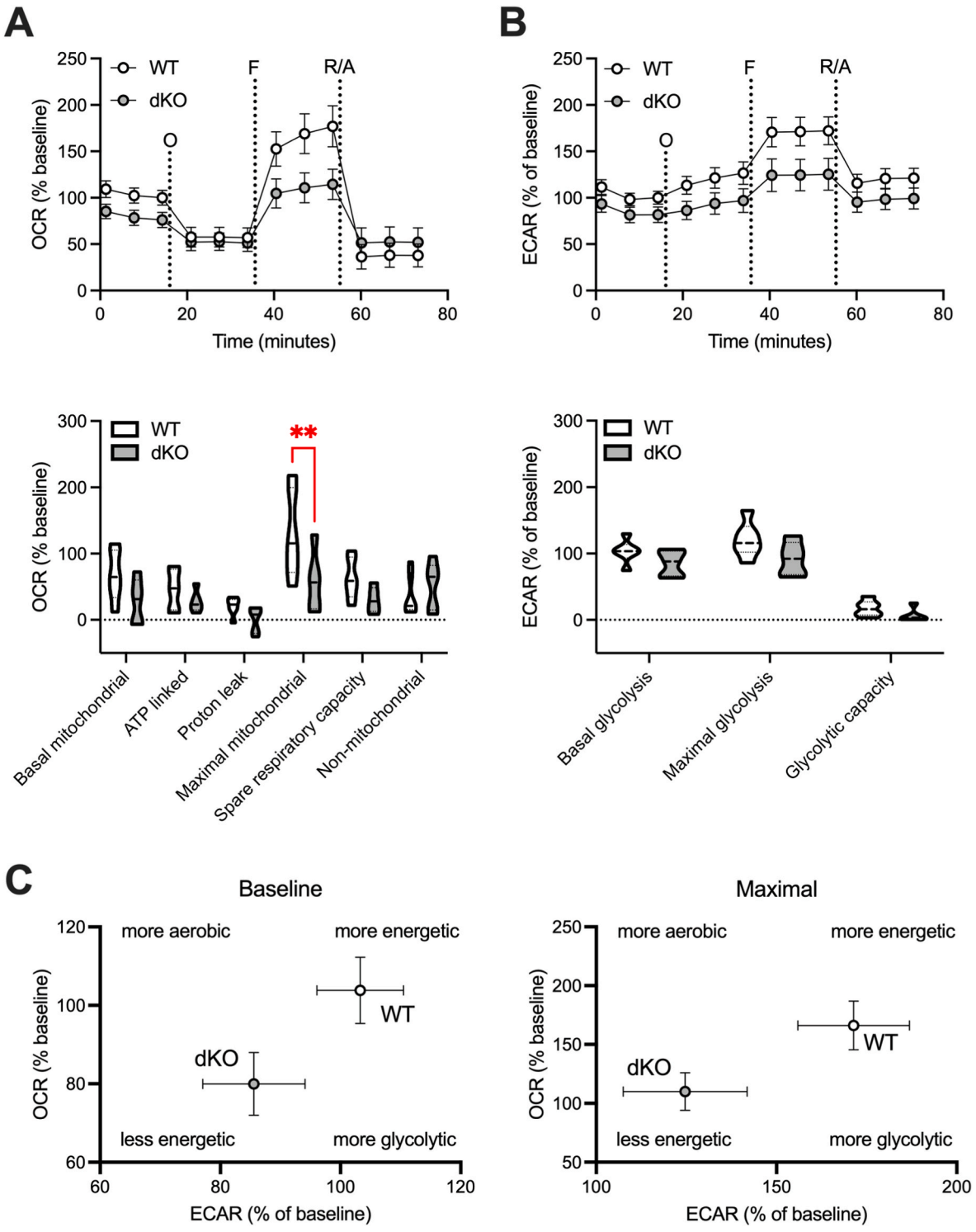

Fig. 10. Impaired mitochondrial respiration in PBMCs isolated from dKO rats at 12 months. Top panel: graphical representation of the OCR (A) and ECAR (B) responses over time. Sequential injections are indicated as O (the ATP synthase inhibitor oligomycin), F (the ATP synthesis uncoupler FCCP), R/A (a mixture of the complex I and III inhibitors rotenone and antimycin A, respectively). Bottom panel: mitochondrial respiratory parameters calculated from the OCR (A) and glycolytic parameters calculated from the ECAR (B). Significant in dKO compared to WT ($n = 5$ per group; $p < 0.01$**) using two-way ANOVA followed by Holm-Sidak multiple comparisons test. (C) Overall energetic phenotype of the PBMCs shown as OCR as a function of ECAR.

only difference in the assessment of rearing frequency between our current study and the previous study was the test apparatus used, which was the cylinder test versus an open field arena, respectively. Using an open field arena to assess rearing at 12 months of age, we found reduced rearing frequency in dKO rats, specifically unsupported rears were affected. Further, we found that open field rearing deficits were responsive to levodopa treatment. Similar to rearing tests in quadruped rodents, the 5 times sit-to-stand test (5xStS) is used to quantify functional lower extremity strength in bipedal humans (Duncan et al., 2011). During the 5xStS, individuals are seated in a chair and then the amount of time it takes for the patients to stand up and sit down five times is recorded. While strength has been thought to be the fundamental

construct influencing 5xStS results, in people with PD, performance on the 5xStS is most related to balance and bradykinesia and can be used to determine whether an individual with PD may be at risk of falling (Duncan et al., 2011). Indeed, populations known to have balance problems including those with PD perform the 5xStS more slowly than healthy older adults (Duncan et al., 2011). As stated above, rearing frequency, particularly unsupported rearing, decreased in dKO rats, reflecting a loss of balance correlating with human PD 5xStS outcomes.

Pink1/Parkin dKO rats exhibit hindlimb dragging in 100% of males and 30% of females. Further, approximately 30% of dams died during childbirth. While we focused here on characterizing the male Pink1/Parkin dKO rats, these findings suggest combined deficiency of Pink1 and Parkin also affects female rats, albeit perhaps without complete penetrance, and as such future studies are warranted. Of note, older male Pink1/Parkin dKO rats weigh more than their WT counterparts, hinting that a metabolic abnormality may develop with aging.

In addition to the hindlimb dragging phenotype, several other qualitative visual observations were made, including observing tremors in the dKO rats while at rest, especially prominent in the forelimbs, lower trunk and flank. Tremor is one of the most visible features of PD, and the typical PD tremor occurs at rest and usually begins in a limb, often in hands or fingers (Heusinkveld et al., 2018). Further, the dKO rats exhibit abnormal movements of the mouth and tongue reminiscent of lingual dyskinesia or lingual protrusion dystonia, which are described in PD patients (Maiola et al., 2016; Sheehy et al., 2008). While rats can't vomit, they can regurgitate, and the dKO rats appear to occasionally undergo retching movements, suggesting they may be experiencing gastroparesis, another symptom in PD. These behaviors appeared at least partially ameliorated by levodopa treatment as the observed frequency and severity was reduced. Future quantitative assessments are warranted.

Coinciding with the motor deficits at 12 months of age, a clear reduction in staining for TH was observed in the SNpc of dKO rats. The cell bodies of the TH-expressing neurons were almost completely absent, with only some remaining axonal projections exiting the SNpc. In addition to reduced TH expression, our study found higher levels of NfL, a marker for neuronal degeneration, in the plasma from the dKO rats compared with age-matched controls. Taken together, these findings reveal loss of TH expressing DA neurons in the SNpc of dKO rats. Elevated plasma NfL levels have been found in PD patients versus control subjects (Pilotto et al., 2021b) and in PD patients with dementia compared to non-demented PD patients (Lin et al., 2018). Additionally, blood NfL concentration can be used to distinguish PD from atypical parkinsonian disorders (Hansson et al., 2017). Further, PD patients with increased plasma NfL exhibit more severe motor and non-motor symptoms, and worse motor progression (Pilotto et al., 2021b). Our findings correlate motor abnormalities with NfL plasma levels in the dKO rats.

PD is known to have a neuroimmune element, with the presence of gliosis from distressed microglia and astrocytes in the brain (Kam et al., 2020). Microglia and astrocytes in the 12-month-old dKO rat brain exhibited morphological changes characteristic of a reactive and/or post-reactive phenotype. In the dKO SNpc, microglia were more amoeboid with less branching when compared to WT rats. The branch retraction of microglia and adoption of an amoeboid cellular shape has been reported to be present in post-mortem brains of PD patients (Doorn et al., 2014a, 2014b). Similar to the microglia, the branching of the astrocytes in the dKO SNpc was extremely retracted exhibiting morphology reminiscent of gemistocytic astrocytes. Gemistocytic astrocytes are thought to be a post-reactive deteriorating stage of astrocyte activation, these are rare and reports on their presence have been limited to certain glioblastomas, some psychiatric disorders, and encephalitis cases (Karnam et al., 2017; Miyahara et al., 2018; Williams et al., 2014). The presence of astroglia atrophy has been reported in some neurodegenerative diseases, including Alzheimer's disease (Verkhratsky et al., 2019); although, to the best of our knowledge, little to no data are available reporting the presence of gemistocytic astrocytes in PD patients, let alone a mammalian model of the disease. Microgliosis and astrocytic gliosis has been reported in human brains with PD-linked PD (Steele et al., 2015). Immunostaining for GFAP has been performed in the SNpc from autopsied brains of three Parkin-mutated patients revealing loss of staining (Kano et al., 2020). This is in line with our finding, since we observe post-reactive deteriorating astroglia in dKO rats. This suggests astrocytes degenerate and are absent from the SNpc at end-stages of the disease. Additional, histological evaluations of post-mortem brains from PD patients harboring Pink1 and/or Parkin mutations might shed light on the role of post-reactive glia in hereditary PD.

Along with DA neuron cell loss, the formation of Lewy bodies primarily composed of α-syn aggregates is a histological hallmark of PD pathology. The dKO rats showed no significant changes in α-syn in the SNpc; however, in the striatum a signal redistribution and formation of α-syn puncta was observed. These findings are similar to those obtained in the Pink1 KO rat, where no α-syn protein level changes were observed but a shift of the protein from the cytosolic fraction towards the synaptic compartment was found in brain homogenates (Creed and Goldberg, 2018). Indeed, α-syn is a presynaptically localized protein, and the SNpc DA nerve synapses are located in the striatum, where we observe α-syn aggregation. Using an aggregation specific α-syn antibody, we confirmed that the observed puncta in the striatum were in fact α-syn aggregates. Increasing evidence suggests aggregation of α-syn at the synapse is an early event in PD pathogenesis and is associated with impaired striatal synaptic function and DA neuronal death (Faustini et al., 2022; Srinivasan et al., 2021). While PD patients with Parkin mutations rarely exhibit Lewy pathology (Schneider and Alcalay, 2017), only seventeen studies published from 1994 to 2018 have investigated post-mortem brains from such patients with a focus on Lewy body formation and of these eight reported the presence of Lewy bodies and one showed basophilic Lewy body-like inclusion bodies (reviewed in (Madsen et al., 2021)). Even less is known about PD patients with Pink1 mutations but reports exist of clear Lewy body pathology at autopsy (Samaranch et al., 2010; Steele et al., 2015). CSF levels of total α-syn have been reported to be lower in patients with PD and dementia with Lewy bodies compared with controls (van Steenoven et al., 2018). Similarly, we found lower levels of α-syn in the CSF from dKO rats. In contrast, we found elevated levels of α-syn in the plasma from dKO rats. Plasma α-syn levels have been found to be higher in PD patients, predict cognitive decline in PD, and moderately correlate with motor severity in patients with early PD (Chang et al., 2019; Lin et al., 2017).

Chronic inflammation is associated with neurodegenerative disorders, including PD and often includes vascular inflammation of the CNS and altered distributions of peripheral blood populations. Our results suggest that loss of Pink1 and Parkin in the dKO model is not associated with significant differences in numbers of peripheral whole blood lymphocytes, leukocytes, or erythrocytes; however, we did observe a significant elevation in the number of platelets that did not coincide with an increase in mean platelet volume. Alterations in platelet dynamics are reported in conjunction with PD clinically yet remain controversial. In one study the reported mean platelet volume was elevated in PD but not AD patients relative to healthy controls, while platelet counts were comparable (Kocer et al., 2013). Conversely, a more recent study reported no significant difference in mean platelet volume in PD patients (Geyik et al., 2016). Both studies reported a significant negative correlation between mean platelet volume and Heohn and Yahr scale score and postulate that inflammation may play an important role in last-stage disease. In addition to altered mean platelet volume, low count, impaired glutamate uptake, reduced monoamine transporter 2 expression, and mitochondrial dysfunction have also been reported in platelets from PD patients (Benecke et al., 1993; Ferrarese et al., 1999; Haas et al., 1995; Sala et al., 2010). Of note, the highest concentration of α-syn per mg of cellular protein in blood is found in these small platelets (Stefaniuk et al., 2022; Tashkandi et al., 2018). Although we did not observe differences in mean platelet volume, our observation of elevated

platelets supports a role for platelet dysfunction in the pathology of PD. Future investigations focusing on a more comprehensive characterization of platelet abnormalities in the dKO model will be of significant interest.

While we did not uncover significant differences in total numbers of leukocytes, we did find that the populations of circulating leukocytes were different in the dKO rats. In particular, we found elevated levels of $CD3^+$ $CD4^+$ T cells and reduced levels of $CD3^+$ $CD8^+$ T cells. Further, we uncovered a significant increase in $CD3^+$ T cell infiltration into the striatum of dKO rats. $CD3^+$ $CD4^+$ and $CD8^+$ T cells, but not B cells, have been identified in brain specimens from individuals with PD (Brochard et al., 2009). T cell involvement in PD has been extensively studied in the MPTP and adeno-associated virus (AAV)-mediated expression of α-syn in mouse models (reviewed in (Baird et al., 2019)). Consistent with evidence that T cells contribute to PD pathogenesis, modulation of T cells in preclinical models can mediate neuroprotection (Benner et al., 2004; Brochard et al., 2009; Kosloski et al., 2013). Pink1 KO mouse T cells have been found to be less effective at suppressing bystander T cell proliferation under conditions favoring Treg polarization (Ellis et al., 2013). Further, a strong inflammatory phenotype has been reported in both Pink1 and Parkin KO mice (Sliter et al., 2018). Intestinal infection with Gram-negative bacteria in Pink1 KO mice leads to brain infiltration by $CD8^+$ T cells (Matheoud et al., 2019). Epidemiological studies have revealed a link of autoimmune disorders with PD (Li et al., 2012). While a paucity of research exists on T cells in genetic PD patients, some of the strongest evidence for T cell involvement in PD pathogenesis have come from recent studies examining autoimmunity to α-syn. Using peptides spanning the α-syn protein, both $CD4^+$ and $CD8^+$ T cell responses could be identified (Lindestam Arlehamn et al., 2020; Sulzer et al., 2017). These responses were especially prominent in $CD4^+$ T cells; and included both T helper 1 (Th1) and Th2 cells. A follow-up study reported last year revealed that T cell responses to α-syn were strongest in the preclinical phase and early in disease onset, and subsequently decreased (Lindestam Arlehamn et al., 2020). In support of α-syn directed $CD4^+$ T cell mediated pathogenesis, in an AAV-expression of α-syn mouse model of PD, MHC (the mouse HLA equivalent) class II was required for disease (Harms et al., 2013). Thus, T cell reactivity to α-syn may represent not only a predictive biomarker, but a potentially modifiable pathogenic mechanism in PD. Taken together, our data suggests the dKO rat model will be invaluable for studying the interplay between α-syn, T cells, and PD pathogenesis.

Pink1 and Parkin mediate mitochondrial quality control, and we found that PBMCs isolated from 12-month-old dKO rats exhibit impaired maximal mitochondrial function while glycolytic function was unaltered. We also note an overall decrease in the energetic status of the PBMCs from the dKO rats at both basal and maximal conditions. PBMCs from young (2–3 months) Pink1 sKO rats showed increased mitochondrial respiration and glycolysis as compared to WT (Grigoruta et al., 2020). Mitochondrial dysfunction in PBMCs has been found in prodromal and early PD patients (Smith et al., 2018). Thus, additional studies will inform on the contribution of peripheral immune cell metabolic changes and relevance to disease progression.

In conclusion, we generated a novel Pink1/Parkin dKO rat, which upon phenotypic characterization was found to reproducibly display pathological features similar to those observed in PD. Motor dysfunction, specifically early gait abnormalities and decreased rearing frequency were present in Pink1/Parkin dKO rats. Pink1/Parkin dKO rats exhibited elevated plasma levels of neurofilament light chain and significant loss of tyrosine hydroxylase expression in the SNpc, suggesting DA neuron loss. Glial cell activation was also observed in the SNpc. Pink1/Parkin dKO rats showed elevated plasma and reduced cerebrospinal levels of α-syn as well as the presence of α-syn aggregates in the striatum. Further, the profile of circulating lymphocytes was altered, as elevated CD3 $CD4^+$ T cells and reduced CD3 $CD8^+$ T cells in Pink1/Parkin dKO rats were found. This coincided with mitochondrial dysfunction and infiltration of $CD3^+$ T cells in the striatum. This model provides an important tool to explore disease pathogenesis and therapeutic strategies for patients with PD and to expand our knowledge about the importance of Pink1/Parkin-dependent mitochondrial quality control within and beyond the brain.

Funding source

This research was funded by Michael J. Fox Foundation for Parkinson's research grant #15288 and the National Institutes of Health Cognitive Neuroscience of Development and Aging (CoNDA) Center grant #1P20 GM130447, Pilot Project.

Declaration of competing interest

The authors declare that they have no known competing financial interests or personal relationships that could have appeared to influence the work reported in this paper.

Data availability

Data will be made available on request.

Acknowledgment

The authors thank Dr. Howard Fox for invaluable scientific input. The graduate studies of Mohannad Almikhlafi were graciously supported by the Saudi Arabian Cultural Mission and Taibah University. We thank the UNMC Flow Cytometry Research Facility.

Appendix A. Supplementary data

Supplementary data to this article can be found online at https://doi.org/10.1016/j.bbih.2023.100656.

References

Backstrom, D., Linder, J., Jakobson Mo, S., Riklund, K., Zetterberg, H., Blennow, K., Forsgren, L., Lenfeldt, N., 2020. NfL as a biomarker for neurodegeneration and survival in Parkinson disease. Neurology 95, e827–e838.

Baird, J.K., Bourdette, D., Meshul, C.K., Quinn, J.F., 2019. The key role of T cells in Parkinson's disease pathogenesis and therapy. Parkinsonism Relat. Disorders 60, 25–31.

Barnett-Vanes, A., Sharrock, A., Birrell, M.A., Rankin, S., 2016. A single 9-colour flow cytometric method to characterise major leukocyte populations in the rat: validation in a model of LPS-induced pulmonary inflammation. PLoS One 11, e0142520.

Benecke, R., Strumper, P., Weiss, H., 1993. Electron transfer complexes I and IV of platelets are abnormal in Parkinson's disease but normal in Parkinson-plus syndromes. Brain 116 (Pt 6), 1451–1463.

Benner, E.J., Mosley, R.L., Destache, C.J., Lewis, T.B., Jackson-Lewis, V., Gorantla, S., Nemachek, C., Green, S.R., Przedborski, S., Gendelman, H.E., 2004. Therapeutic immunization protects dopaminergic neurons in a mouse model of Parkinson's disease. Proc. Natl. Acad. Sci. U. S. A. 101, 9435–9440.

Brochard, V., Combadiere, B., Prigent, A., Laouar, Y., Perrin, A., Beray-Berthat, V., Bonduelle, O., Alvarez-Fischer, D., Callebert, J., Launay, J.M., Duyckaerts, C., Flavell, R.A., Hirsch, E.C., Hunot, S., 2009. Infiltration of CD4+ lymphocytes into the brain contributes to neurodegeneration in a mouse model of Parkinson disease. J. Clin. Invest. 119, 182–192.

Broom, L., Ellison, B.A., Worley, A., Wagenaar, L., Sorberg, E., Ashton, C., Bennett, D.A., Buchman, A.S., Saper, C.B., Shih, L.C., Hausdorff, J.M., VanderHorst, V.G., 2017. A translational approach to capture gait signatures of neurological disorders in mice and humans. Sci. Rep. 7, 3225.

Broom, L., Stephen, J., Nayar, V., VanderHorst, V.G., 2021. Shifts in gait signatures mark the end of lifespan in mice, with sex differences in timing. Front. Aging Neurosci. 13, 716993.

Canaslan, S., Schmitz, M., Villar-Pique, A., Maass, F., Gmitterova, K., Varges, D., Lingor, P., Llorens, F., Hermann, P., Zerr, I., 2021. Detection of cerebrospinal fluid neurofilament light chain as a marker for alpha-synucleinopathies. Front. Aging Neurosci. 13, 717930.

Chang, C.W., Yang, S.Y., Yang, C.C., Chang, C.W., Wu, Y.R., 2019. Plasma and serum alpha-synuclein as a biomarker of diagnosis in patients with Parkinson's disease. Front. Neurol. 10, 1388.

Clark, I.E., Dodson, M.W., Jiang, C., Cao, J.H., Huh, J.R., Seol, J.H., Yoo, S.J., Hay, B.A., Guo, M., 2006. Drosophila pink1 is required for mitochondrial function and interacts genetically with parkin. Nature 441, 1162–1166.

Creed, R.B., Goldberg, M.S., 2018. Analysis of alpha-synuclein pathology in PINK1 knockout rat brains. Front. Neurosci. 12, 1034.
Creed, R.B., Menalled, L., Casey, B., Dave, K.D., Janssens, H.B., Veinbergs, I., van der Hart, M., Rassoulpour, A., Goldberg, M.S., 2019. Basal and evoked neurotransmitter levels in parkin, DJ-1, PINK1 and LRRK2 knockout rat striatum. Neuroscience 409, 169–179.
Dave, K.D., De Silva, S., Sheth, N.P., Ramboz, S., Beck, M.J., Quang, C., Switzer 3rd, R.C., Ahmad, S.O., Sunkin, S.M., Walker, D., Cui, X., Fisher, D.A., McCoy, A.M., Gamber, K., Ding, X., Goldberg, M.S., Benkovic, S.A., Haupt, M., Baptista, M.A., Fiske, B.K., Sherer, T.B., Frasier, M.A., 2014. Phenotypic characterization of recessive gene knockout rat models of Parkinson's disease. Neurobiol. Dis. 70, 190–203.
de Haas, R., Heltzel, L., Tax, D., van den Broek, P., Steenbreker, H., Verheij, M.M.M., Russel, F.G.M., Orr, A.L., Nakamura, K., Smeitink, J.A.M., 2019. To be or not to be pink(1): contradictory findings in an animal model for Parkinson's disease. Brain Commun 1, fcz016.
DeAngelo, V.M., Hilliard, J.D., McConnell, G.C., 2022. Dopaminergic but not cholinergic neurodegeneration is correlated with gait disturbances in PINK1 knockout rats. Behav. Brain Res. 417, 113575.
Doorn, K.J., Goudriaan, A., Blits-Huizinga, C., Bol, J.G., Rozemuller, A.J., Hoogland, P. V., Lucassen, P.J., Drukarch, B., van de Berg, W.D., van Dam, A.M., 2014a. Increased amoeboid microglial density in the olfactory bulb of Parkinson's and Alzheimer's patients. Brain Pathol. 24, 152–165.
Doorn, K.J., Moors, T., Drukarch, B., van de Berg, W., Lucassen, P.J., van Dam, A.M., 2014b. Microglial phenotypes and toll-like receptor 2 in the substantia nigra and hippocampus of incidental Lewy body disease cases and Parkinson's disease patients. Acta Neuropathol. Commun. 2, 90.
Duncan, R.P., Leddy, A.L., Earhart, G.M., 2011. Five times sit-to-stand test performance in Parkinson's disease. Arch. Phys. Med. Rehabil. 92, 1431–1436.
Ellis, G.I., Zhi, L., Akundi, R., Bueler, H., Marti, F., 2013. Mitochondrial and cytosolic roles of PINK1 shape induced regulatory T-cell development and function. Eur. J. Immunol. 43, 3355–3360.
Exner, N., Lutz, A.K., Haass, C., Winklhofer, K.F., 2012. Mitochondrial dysfunction in Parkinson's disease: molecular mechanisms and pathophysiological consequences. EMBO J. 31, 3038–3062.
Faustini, G., Longhena, F., Masato, A., Bassareo, V., Frau, R., Klingstedt, T., Shirani, H., Brembati, V., Parrella, E., Vezzoli, M., Nilsson, K.P.R., Pizzi, M., Spillantini, M.G., Bubacco, L., Bellucci, A., 2022. Synapsin III gene silencing redeems alpha-synuclein transgenic mice from Parkinson's disease-like phenotype. Mol. Ther. 30, 1465–1483.
Ferrarese, C., Zoia, C., Pecora, N., Piolti, R., Frigo, M., Bianchi, G., Sala, G., Begni, B., Riva, R., Frattola, L., 1999. Reduced platelet glutamate uptake in Parkinson's disease. J. Neural. Transm. 106, 685–692.
Funayama, M., Li, Y., Tsoi, T.H., Lam, C.W., Ohi, T., Yazawa, S., Uyama, E., Djaldetti, R., Melamed, E., Yoshino, H., Imamichi, Y., Takashima, H., Nishioka, K., Sato, K., Tomiyama, H., Kubo, S., Mizuno, Y., Hattori, N., 2008. Familial Parkinsonism with digenic parkin and PINK1 mutations. Mov. Disord. 23, 1461–1465.
Geyik, S., Y, R., Akgul, G.P., Elci, M., Firat, Y.E., 2016. The relationship between Parkinson's disease and mean platelet volume. Park. Hast. Hareket Bozukluklari Derg 19, 31–34.
Gispert, S., Ricciardi, F., Kurz, A., Azizov, M., Hoepken, H.H., Becker, D., Voos, W., Leuner, K., Muller, W.E., Kudin, A.P., Kunz, W.S., Zimmermann, A., Roeper, J., Wenzel, D., Jendrach, M., Garcia-Arencibia, M., Fernandez-Ruiz, J., Huber, L., Rohrer, H., Barrera, M., Reichert, A.S., Rub, U., Chen, A., Nussbaum, R.L., Auburger, G., 2009. Parkinson phenotype in aged PINK1-deficient mice is accompanied by progressive mitochondrial dysfunction in absence of neurodegeneration. PLoS One 4, e5777.
Goldberg, M.S., Fleming, S.M., Palacino, J.J., Cepeda, C., Lam, H.A., Bhatnagar, A., Meloni, E.G., Wu, N., Ackerson, L.C., Klapstein, G.J., Gajendiran, M., Roth, B.L., Chesselet, M.F., Maidment, N.T., Levine, M.S., Shen, J., 2003. Parkin-deficient mice exhibit nigrostriatal deficits but not loss of dopaminergic neurons. J. Biol. Chem. 278, 43628–43635.
Grant, L.M., Kelm-Nelson, C.A., Hilby, B.L., Blue, K.V., Paul Rajamanickam, E.S., Pultorak, J.D., Fleming, S.M., Ciucci, M.R., 2015. Evidence for early and progressive ultrasonic vocalization and oromotor deficits in a PINK1 gene knockout rat model of Parkinson's disease. J. Neurosci. Res. 93, 1713–1727.
Greene, J.C., Whitworth, A.J., Kuo, I., Andrews, L.A., Feany, M.B., Pallanck, L.J., 2003. Mitochondrial pathology and apoptotic muscle degeneration in Drosophila parkin mutants. Proc. Natl. Acad. Sci. U. S. A. 100, 4078–4083.
Grigoruta, M., Dagda, R.K., Diaz-Sanchez, A.G., Martinez-Martinez, A., 2020. Psychological distress and lack of PINK1 promote bioenergetics alterations in peripheral blood mononuclear cells. Sci. Rep. 10, 9820.
Grigoryan, G., Hodges, H., Mitchell, S., Sinden, J.D., Gray, J.A., 1996. 6-OHDA lesions of the nucleus accumbens accentuate memory deficits in animals with lesions to the forebrain cholinergic projection system: effects of nicotine administration on learning and memory in the water maze. Neurobiol. Learn. Mem. 65, 135–153.
Haas, R.H., Nasirian, F., Nakano, K., Ward, D., Pay, M., Hill, R., Shults, C.W., 1995. Low platelet mitochondrial complex I and complex II/III activity in early untreated Parkinson's disease. Ann. Neurol. 37, 714–722.
Hansson, O., Janelidze, S., Hall, S., Magdalinou, N., Lees, A.J., Andreasson, U., Norgren, N., Linder, J., Forsgren, L., Constantinescu, R., Zetterberg, H., Blennow, K., Swedish Bio, F.s., 2017. Blood-based NfL: a biomarker for differential diagnosis of parkinsonian disorder. Neurology 88, 930–937.
Harms, A.S., Cao, S., Rowse, A.L., Thome, A.D., Li, X., Mangieri, L.R., Cron, R.Q., Shacka, J.J., Raman, C., Standaert, D.G., 2013. MHCII is required for alpha-synuclein-induced activation of microglia, CD4 T cell proliferation, and dopaminergic neurodegeneration. J. Neurosci. 33, 9592–9600.
Heusinkveld, L.E., Hacker, M.L., Turchan, M., Davis, T.L., Charles, D., 2018. Impact of tremor on patients with early stage Parkinson's disease. Front. Neurol. 9, 628.
Hirsch, L., Jette, N., Frolkis, A., Steeves, T., Pringsheim, T., 2016. The incidence of Parkinson's disease: a systematic review and meta-analysis. Neuroepidemiology 46, 292–300.
Itier, J.M., Ibanez, P., Mena, M.A., Abbas, N., Cohen-Salmon, C., Bohme, G.A., Laville, M., Pratt, J., Corti, O., Pradier, L., Ret, G., Joubert, C., Periquet, M., Araujo, F., Negroni, J., Casarejos, M.J., Canals, S., Solano, R., Serrano, A., Gallego, E., Sanchez, M., Denefle, P., Benavides, J., Tremp, G., Rooney, T.A., Brice, A., Garcia de Yebenes, J., 2003. Parkin gene inactivation alters behaviour and dopamine neurotransmission in the mouse. Hum. Mol. Genet. 12, 2277–2291.
Kam, T.I., Hinkle, J.T., Dawson, T.M., Dawson, V.L., 2020. Microglia and astrocyte dysfunction in Parkinson's disease. Neurobiol. Dis. 144, 105028.
Kano, M., Takanashi, M., Oyama, G., Yoritaka, A., Hatano, T., Shiba-Fukushima, K., Nagai, M., Nishiyama, K., Hasegawa, K., Inoshita, T., Ishikawa, K.I., Akamatsu, W., Imai, Y., Bolognin, S., Schwamborn, J.C., Hattori, N., 2020. Reduced astrocytic reactivity in human brains and midbrain organoids with PRKN mutations. NPJ Parkinsons Dis. 6, 33.
Karnam, S., Kottu, R., Chowhan, A.K., Bodepati, P.C., 2017. Expression of p53 & epidermal growth factor receptor in glioblastoma. Indian J. Med. Res. 146, 738–745.
Kelm-Nelson, C.A., Lechner, S.A., Lettenberger, S.E., Kaldenberg, T.A.R., Pahapill, N.K., Regenbaum, A., Ciucci, M.R., 2021. Pink1(-/-) rats are a useful tool to study early Parkinson disease. Brain Commun 3, fcab077.
Kitada, T., Pisani, A., Porter, D.R., Yamaguchi, H., Tscherter, A., Martella, G., Bonsi, P., Zhang, C., Pothos, E.N., Shen, J., 2007. Impaired dopamine release and synaptic plasticity in the striatum of PINK1-deficient mice. Proc. Natl. Acad. Sci. U. S. A. 104, 11441–11446.
Kitada, T., Tong, Y., Gautier, C.A., Shen, J., 2009. Absence of nigral degeneration in aged parkin/DJ-1/PINK1 triple knockout mice. J. Neurochem. 111, 696–702.
Klein, C., Westenberger, A., 2012. Genetics of Parkinson's disease. Cold Spring Harb Perspect. Med. 2, a008888.
Klemann, C., Martens, G.J.M., Poelmans, G., Visser, J.E., 2016. Validity of the MPTP-treated mouse as a model for Parkinson's disease. Mol. Neurobiol. 53, 1625–1636.
Kline, E.M., Houser, M.C., Herrick, M.K., Seibler, P., Klein, C., West, A., Tansey, M.G., 2021. Genetic and environmental factors in Parkinson's disease converge on immune function and inflammation. Mov. Disord. 36, 25–36.
Kocer, A., Yaman, A., Niftaliyev, E., Duruyen, H., Eryilmaz, M., Kocer, E., 2013. Assessment of platelet indices in patients with neurodegenerative diseases: mean platelet volume was increased in patients with Parkinson's disease. Curr Gerontol Geriatr Res 2013, 986254.
Kosloski, L.M., Kosmacek, E.A., Olson, K.E., Mosley, R.L., Gendelman, H.E., 2013. GM-CSF induces neuroprotective and anti-inflammatory responses in 1-methyl-4-phenyl-1,2,3,6-tetrahydropyridine intoxicated mice. J. Neuroimmunol. 265, 1–10.
Lesage, S., Houot, M., Mangone, G., Tesson, C., Bertrand, H., Forlani, S., Anheim, M., Brefel-Courbon, C., Broussolle, E., Thobois, S., Damier, P., Durif, F., Roze, E., Tison, F., Grabli, D., Ory-Magne, F., Degos, B., Viallet, F., Cormier-Dequaire, F., Ouvrard-Hernandez, A.M., Vidailhet, M., Lohmann, E., Singleton, A., Corvol, J.C., Brice, A., French Parkinson disease Genetics Study, G., 2020. Genetic and phenotypic basis of autosomal dominant Parkinson's disease in a large multi-center cohort. Front. Neurol. 11, 682.
Li, X., Sundquist, J., Sundquist, K., 2012. Subsequent risks of Parkinson disease in patients with autoimmune and related disorders: a nationwide epidemiological study from Sweden. Neurodegener. Dis. 10, 277–284.
Lin, C.H., Yang, S.Y., Horng, H.E., Yang, C.C., Chieh, J.J., Chen, H.H., Liu, B.H., Chiu, M. J., 2017. Plasma alpha-synuclein predicts cognitive decline in Parkinson's disease. J. Neurol. Neurosurg. Psychiatry 88, 818–824.
Lin, Y.S., Lee, W.J., Wang, S.J., Fuh, J.L., 2018. Levels of plasma neurofilament light chain and cognitive function in patients with Alzheimer or Parkinson disease. Sci. Rep. 8, 17368.
Lindestam Arlehamn, C.S., Dhanwani, R., Pham, J., Kuan, R., Frazier, A., Rezende Dutra, J., Phillips, E., Mallal, S., Roederer, M., Marder, K.S., Amara, A.W., Standaert, D.G., Goldman, J.G., Litvan, I., Peters, B., Sulzer, D., Sette, A., 2020. alpha-Synuclein-specific T cell reactivity is associated with preclinical and early Parkinson's disease. Nat. Commun. 11, 1875.
Madsen, D.A., Schmidt, S.I., Blaabjerg, M., Meyer, M., 2021. Interaction between parkin and alpha-synuclein in PARK2-mediated Parkinson's disease. Cells 10.
Maiola, R., Ramirez Gomez, C.C., Micheli, F., 2016. Lingual protrusion dystonia: manifestation during "on" periods in Parkinson's disease. J. Neurol. Sci. 370, 256–257.
Matheoud, D., Cannon, T., Voisin, A., Penttinen, A.M., Ramet, L., Fahmy, A.M., Ducrot, C., Laplante, A., Bourque, M.J., Zhu, L., Cayrol, R., Le Campion, A., McBride, H.M., Gruenheid, S., Trudeau, L.E., Desjardins, M., 2019. Intestinal infection triggers Parkinson's disease-like symptoms in Pink1(-/-) mice. Nature 571, 565–569.
Mendes, C.S., Bartos, I., Marka, Z., Akay, T., Marka, S., Mann, R.S., 2015. Quantification of gait parameters in freely walking rodents. BMC Biol. 13, 50.
Miller, D.B., O'Callaghan, J.P., 2015. Biomarkers of Parkinson's disease: present and future. Metabolism 64, S40–S46.
Miyahara, H., Miyakawa, K., Nishida, H., Yano, S., Sonoda, T., Suenobu, S.I., Izumi, T., Daa, T., Ihara, K., 2018. Unique cell tropism of HHV-6B in an infantile autopsy case of primary HHV-6B encephalitis. Neuropathology.
Orr, A.L., Rutaganira, F.U., de Roulet, D., Huang, E.J., Hertz, N.T., Shokat, K.M., Nakamura, K., 2017. Long-term oral kinetin does not protect against alpha-synuclein-induced neurodegeneration in rodent models of Parkinson's disease. Neurochem. Int. 109, 106–116.

Park, J., Lee, S.B., Lee, S., Kim, Y., Song, S., Kim, S., Bae, E., Kim, J., Shong, M., Kim, J. M., Chung, J., 2006. Mitochondrial dysfunction in Drosophila PINK1 mutants is complemented by parkin. Nature 441, 1157–1161.
Pickles, S., Vigie, P., Youle, R.J., 2018. Mitophagy and quality control mechanisms in mitochondrial maintenance. Curr. Biol. 28, R170–R185.
Pilotto, A., Imarisio, A., Carrarini, C., Russo, M., Masciocchi, S., Gipponi, S., Cottini, E., Aarsland, D., Zetterberg, H., Ashton, N.J., Hye, A., Bonanni, L., Padovani, A., 2021a. Plasma neurofilament light chain predicts cognitive progression in prodromal and clinical dementia with lewy bodies. J. Alzheimers Dis. 82, 913–919.
Pilotto, A., Imarisio, A., Conforti, F., Scalvini, A., Masciocchi, S., Nocivelli, S., Turrone, R., Gipponi, S., Cottini, E., Borroni, B., Rizzetti, M.C., Pizzi, M., Bonanni, L., Sturchio, A., Espay, A.J., Zetterberg, H., Ashton, N.J., Hye, A., Padovani, A., 2021b. Plasma NfL, clinical subtypes and motor progression in Parkinson's disease. Parkinsonism Relat. Disorders 87, 41–47.
Quadalti, C., Calandra-Buonaura, G., Baiardi, S., Mastrangelo, A., Rossi, M., Zenesini, C., Giannini, G., Candelise, N., Sambati, L., Polischi, B., Plazzi, G., Capellari, S., Cortelli, P., Parchi, P., 2021. Neurofilament light chain and alpha-synuclein RT-QuIC as differential diagnostic biomarkers in parkinsonisms and related syndromes. NPJ Parkinsons Dis. 7, 93.
Sala, G., Brighina, L., Saracchi, E., Fermi, S., Riva, C., Carrozza, V., Pirovano, M., Ferrarese, C., 2010. Vesicular monoamine transporter 2 mRNA levels are reduced in platelets from patients with Parkinson's disease. J. Neural. Transm. 117, 1093–1098.
Samaranch, L., Lorenzo-Betancor, O., Arbelo, J.M., Ferrer, I., Lorenzo, E., Irigoyen, J., Pastor, M.A., Marrero, C., Isla, C., Herrera-Henriquez, J., Pastor, P., 2010. PINK1-linked parkinsonism is associated with Lewy body pathology. Brain 133, 1128–1142.
Schneider, S.A., Alcalay, R.N., 2017. Neuropathology of genetic synucleinopathies with parkinsonism: review of the literature. Mov. Disord. 32, 1504–1523.
Sheehy, S.H., Lawrence, T., Thevathasan, A.W., 2008. Serpentine tongue: a lingual dyskinesia. Neurology 70, e87.
Sliter, D.A., Martinez, J., Hao, L., Chen, X., Sun, N., Fischer, T.D., Burman, J.L., Li, Y., Zhang, Z., Narendra, D.P., Cai, H., Borsche, M., Klein, C., Youle, R.J., 2018. Parkin and PINK1 mitigate STING-induced inflammation. Nature 561, 258–262.
Smith, A.M., Depp, C., Ryan, B.J., Johnston, G.I., Alegre-Abarrategui, J., Evetts, S., Rolinski, M., Baig, F., Ruffmann, C., Simon, A.K., Hu, M.T.M., Wade-Martins, R., 2018. Mitochondrial dysfunction and increased glycolysis in prodromal and early Parkinson's blood cells. Mov. Disord. 33, 1580–1590.
Srinivasan, E., Chandrasekhar, G., Chandrasekar, P., Anbarasu, K., Vickram, A.S., Karunakaran, R., Rajasekaran, R., Srikumar, P.S., 2021. Alpha-synuclein aggregation in Parkinson's disease. Front. Med. 8, 736978.
Stauch, K.L., Totusek, S., Farmer, T., Lamberty, B.G., Dyball, K.N., Almikhlafi, M.A., Fox, H.S., 2021. Applying the RatWalker system for gait analysis in a genetic rat model of Parkinson's disease. J. Vis. Exp. 167.
Steele, J.C., Guella, I., Szu-Tu, C., Lin, M.K., Thompson, C., Evans, D.M., Sherman, H.E., Vilarino-Guell, C., Gwinn, K., Morris, H., Dickson, D.W., Farrer, M.J., 2015. Defining neurodegeneration on Guam by targeted genomic sequencing. Ann. Neurol. 77, 458–468.
Stefaniuk, C.M., Schlegelmilch, J., Meyerson, H.J., Harding, C.V., Maitta, R.W., 2022. Initial assessment of alpha-synuclein structure in platelets. J. Thromb. Thrombolysis 53, 950–953.
Sulzer, D., Alcalay, R.N., Garretti, F., Cote, L., Kanter, E., Agin-Liebes, J., Liong, C., McMurtrey, C., Hildebrand, W.H., Mao, X., Dawson, V.L., Dawson, T.M., Oseroff, C., Pham, J., Sidney, J., Dillon, M.B., Carpenter, C., Weiskopf, D., Phillips, E., Mallal, S., Peters, B., Frazier, A., Lindestam Arlehamn, C.S., Sette, A., 2017. T cells from patients with Parkinson's disease recognize alpha-synuclein peptides. Nature 546, 656–661.
Tashkandi, H., Shameli, A., Harding, C.V., Maitta, R.W., 2018. Ultrastructural changes in peripheral blood leukocytes in alpha-synuclein knockout mice. Blood Cells Mol. Dis. 73, 33–37.
van Steenoven, I., Majbour, N.K., Vaikath, N.N., Berendse, H.W., van der Flier, W.M., van de Berg, W.D.J., Teunissen, C.E., Lemstra, A.W., El-Agnaf, O.M.A., 2018. alpha-Synuclein species as potential cerebrospinal fluid biomarkers for dementia with lewy bodies. Mov. Disord. 33, 1724–1733.
Verkhratsky, A., Rodrigues, J.J., Pivoriunas, A., Zorec, R., Semyanov, A., 2019. Astroglial atrophy in Alzheimer's disease. Pflügers Archiv 471, 1247–1261.
Villeneuve, L.M., Purnell, P.R., Boska, M.D., Fox, H.S., 2016. Early expression of Parkinson's disease-related mitochondrial abnormalities in PINK1 knockout rats. Mol. Neurobiol. 53, 171–186.
Von Coelln, R., Thomas, B., Savitt, J.M., Lim, K.L., Sasaki, M., Hess, E.J., Dawson, V.L., Dawson, T.M., 2004. Loss of locus coeruleus neurons and reduced startle in parkin null mice. Proc. Natl. Acad. Sci. U. S. A. 101, 10744–10749.
Whitworth, A.J., Theodore, D.A., Greene, J.C., Benes, H., Wes, P.D., Pallanck, L.J., 2005. Increased glutathione S-transferase activity rescues dopaminergic neuron loss in a Drosophila model of Parkinson's disease. Proc. Natl. Acad. Sci. U. S. A. 102, 8024–8029.
Williams, M., Pearce, R.K., Hirsch, S.R., Ansorge, O., Thom, M., Maier, M., 2014. Fibrillary astrocytes are decreased in the subgenual cingulate in schizophrenia. Eur. Arch. Psychiatr. Clin. Neurosci. 264, 357–362.
Zanardi, A.P.J., da Silva, E.S., Costa, R.R., Passos-Monteiro, E., Dos Santos, I.O., Kruel, L. F.M., Peyre-Tartaruga, L.A., 2021. Gait parameters of Parkinson's disease compared with healthy controls: a systematic review and meta-analysis. Sci. Rep. 11, 752.